Article

Cell

Metastatic Latency and Immune Evasion through Autocrine Inhibition of WNT

Graphical Abstract

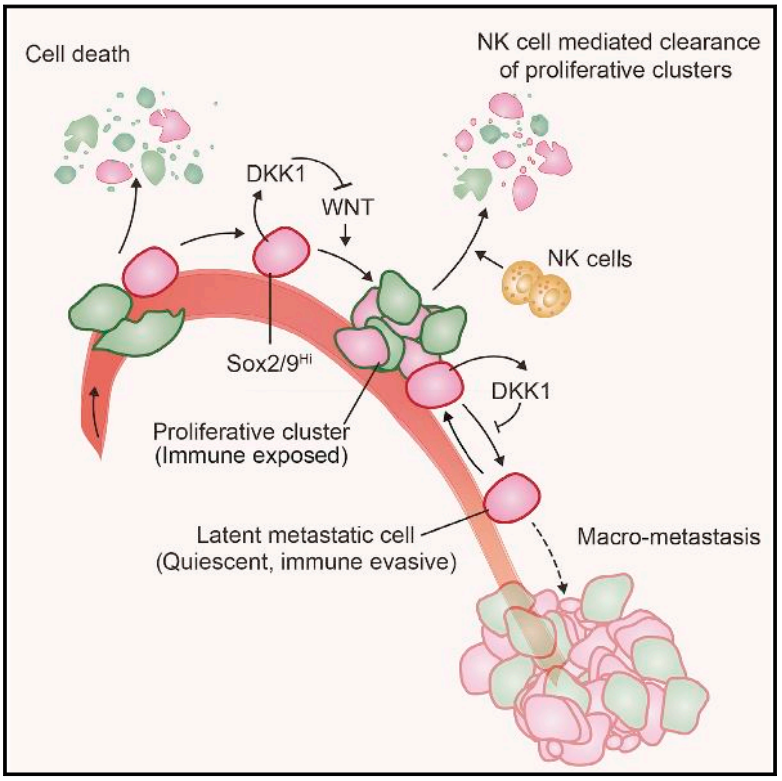

Authors

Srinivas Malladi, Danilo G. Macalinao, Xin Jin, ..., Yilong Zou, Elisa de Stanchina, Joan Massagué

Correspondence

j-massague@ski.mskcc.org

In Brief

The latency and immune evasion of metastatic cancer cells is controlled by autocrine WNT inhibition, which imposes a slow-cycling stem-cell-like state and enables downregulation of cell surface innate immune sensors.

Highlights

- Latency competent cancer (LCC) cells are enriched for SOX transcription factors
- Autocrine WNT inhibition through DKK1 imposes a slow-cycling state in LCC cells
- Slow-cycling state enables downregulation of cell-surface-innate immune sensors
- LCC cells persist long term by evading NK-cell-mediated immune surveillance

Accession Numbers

GSE72956

Malladi et al., 2016, Cell *165*, 45–60
March 24, 2016
http://dx.doi.org/10.1016/j.cell.2016.02.025

CellPress

Cell

Metastatic Latency and Immune Evasion through Autocrine Inhibition of WNT

Srinivas Malladi,[1] Danilo G. Macalinao,[1,2] Xin Jin,[1,4] Lan He,[1] Harihar Basnet,[1] Yilong Zou,[1,2] Elisa de Stanchina,[3] and Joan Massagué[1,*]
[1]Cancer Biology and Genetics Program
[2]Gerstner Sloan Kettering Graduate School of Biomedical Sciences
[3]Antitumor Assessment Core
Memorial Sloan Kettering Cancer Center, New York, NY 10065, USA
[4]Present address: Cancer Program, The Eli and Edythe L. Broad Institute, Cambridge, MA 02142, USA
*Correspondence: j-massague@ski.mskcc.org
http://dx.doi.org/10.1016/j.cell.2016.02.025

SUMMARY

Metastasis frequently develops years after the removal of a primary tumor, from a minority of disseminated cancer cells that survived as latent entities through unknown mechanisms. We isolated latency competent cancer (LCC) cells from early stage human lung and breast carcinoma cell lines and defined the mechanisms that suppress outgrowth, support long-term survival, and maintain tumor-initiating potential in these cells during the latent metastasis stage. LCC cells show stem-cell-like characteristics and express SOX2 and SOX9 transcription factors, which are essential for their survival in host organs under immune surveillance and for metastatic outgrowth under permissive conditions. Through expression of the WNT inhibitor DKK1, LCC cells self-impose a slow-cycling state with broad downregulation of ULBP ligands for NK cells and evasion of NK-cell-mediated clearance. By expressing a Sox-dependent stem-like state and actively silencing WNT signaling, LCC cells can enter quiescence and evade innate immunity to remain latent for extended periods.

INTRODUCTION

Cancer patients with no clinical evidence of disease after the initial treatment frequently relapse with distant metastasis years later. Prior to diagnosis and treatment, primary tumors may release large numbers of cancer cells into the circulation. Although a majority of the dispersed cells perish in the bloodstream or soon after infiltrating distant organs, a minority may survive as latent seeds in host tissues. As a result, people who are clinically considered disease-free after cancer treatment may carry thousands of disseminated tumor cells (DTCs) in the bone marrow and other organs (Braun et al., 2005). Latent metastasis is a major concern in the clinic, yet little is known about the nature of dormant DTCs and the mechanisms that allow these cells to remain quiescent, evade immunity, retain tumor-initiating capacity, and evolve into aggressive metastasis (Massagué and Obenauf, 2016).

A leading hypothesis posits that dormant DTCs are tumor-initiating cells that enter quiescence by the action of growth inhibitory signals from the host tissue stroma (Sosa et al., 2014). Recent studies have identified stromal TGF-β and BMP as inhibitors of DTC growth (Bragado et al., 2013; Gao et al., 2012; Kobayashi et al., 2011). However, organs that host DTCs, such as the bone marrow, liver, and lungs, support cell proliferation as part of their normal tissue homeostasis and regenerative processes, raising questions as to whether stromal growth inhibitory signals are persistent enough to enforce long-term metastatic latency.

Another important consideration is the role of immunity in latent metastasis. The interplay between cancer cells and the various components of the immune system plays a crucial role in tumor progression (Dunn et al., 2004; Eyles et al., 2010; Kitamura et al., 2015). Notably, organ transplants from donors who had been cured of melanoma, or who suffered glioblastoma, considered a non-metastatic tumor, developed donor-derived metastasis in immunosuppressed recipients, suggesting that immune surveillance prevents the outgrowth of dormant DTCs (MacKie et al., 2003; Xiao et al., 2013). Metastatic latency may therefore require DTCs to be in equilibrium with the immune system.

Our understanding of the molecular basis for latent metastasis has been limited by a scarcity of preclinical models that recapitulate key features of this metastatic stage (Massagué and Obenauf, 2016). To address this problem, we isolated latency competent cancer (LCC) cells by in vivo selection of human tumor cell populations in mice. Using these models, we show that LCC cells are a distinct class of stem-like cells primed to enter quiescence and evade innate immunity. LCC cells express SOX transcription factors that impart tumor-initiating stem/progenitor cell identity. These cells can actively self-impose a slow-cycling state by producing DKK1, an inhibitor of the WNT signaling pathway. We propose a quiescence-linked mechanism for evasion of NK-cell-mediated immunity, long-term survival, and evolution of latent metastasis-initiating cells.

RESULTS

Latency Competent Cells Isolated from Early Stage Breast and Lung Cancers

We isolated cancer cells that are competent to seed relevant organs with latent metastasis (latency competent cancer cells, LCC cells). As sources, we used H2087, a cell line derived from stage I lung adenocarcinoma (Gazdar and Minna, 1996), and HCC1954 from a stage IIA HER2$^+$ breast tumor (Gazdar et al., 1998) (Figure S1A). Nearly half of early stage lung adenocarcinoma cases develop distant relapse despite surgical resection of the primary tumor, implying latent disseminated disease (Maeda et al., 2010). The HER2$^+$ breast cancer patient population is experiencing a marked increase in the incidence of brain metastasis after anti-HER2 therapies that suppress extracranial relapse and extend survival (Duchnowska et al., 2009). Thus, both cancer types are important sources of latent metastasis in the clinic.

H2087 and HCC1954 cells transduced with a GFP-luciferase reporter and antibiotic resistance vectors were intracardially injected into the arterial circulation of *FOXN1^{nu}* mice (Pelleitier and Montplaisir, 1975). As monitored by bioluminescence imaging (BLI), most mice remained signal-free and healthy for 3 months. Organs from these mice were dissociated into single-cell suspensions in culture to recover antibiotic-resistant cancer cells from lungs (H2087-LCC1 cell line) and kidneys (H2087-LCC2) of mice injected with H2087 and from brain of mice injected with HCC1954 (HCC1954-LCC1) (Figures S1A and S1B). The tumorigenic activity of LCC cells after orthotopic implantation was similar to that of the parental populations (Figures S1C and S1D). Thus, LCC cells retained tumor-initiating potential after months of latency in mouse tissues.

Of 20 athymic mice injected with H2087-LCC cells, one developed overt metastasis, one a spinal metastasis after 4 months that did not progress, two developed incipient lesions after 7 months, and 16 remained metastasis-free for over 8 months (Figures 1A and 1C). Only one of eight mice injected with HCC1954-LCC1 developed overt metastasis over 4 months (Figures 1B and C). In comparison, aggressive breast (MDA-MB-231) and lung adenocarcinoma (H2030) metastatic lines formed extensive metastases within 3 weeks (Figures 1A, 1B, and S1E).

We were able to histologically detect and recover cancer cells from 20 of 26 (77%) LCC-injected mice that remained metastasis-free, but only from 2 of 14 (14%) mice injected with the parental lines (Figure S1F). H2087-LCC1 and H2087-LCC2 cells targeted both the lungs and the kidneys, suggesting that the latent phenotype of these cells was not strictly organ-specific (Figures 1D–1G). Cells isolated from rare macrometastatic tumors arising in LCC-injected mice (LCC-M lines) showed a latent phenotype upon reinjection, with no increase in macrometastatic activity, arguing that LCC cells stochastically form overt metastases (Figure S1G).

LCC Cell Localization in Infiltrated Organs

We chose H2087-LCC1, H2087-LCC2, HCC1954-LCC1, and the HCC1954-LCC2 lines derived from LCC1-injected mice for further analysis. Two weeks after inoculation, ~20% of disseminated GFP$^+$ HCC1954 LCC cells in the brain were found in small clusters (>10 cells) and the rest as single cells (Figure S1H). After 3 months, more than 90% of the GFP$^+$ DTCs were found as single cells and the rest as small clusters of ~20 cells, as determined by anti-GFP immunostaining (Figures 1D and 1E), H&E staining (Figure 1F), and human vimentin immunostaining (Figure 1G).

In the kidney, LCC cells were detected between the renal tubules, adjacent to capillaries, or within glomeruli (Figures 1F and 1G). A few LCC cells were observed within the adrenal gland cortex (Figure S1I). In the lungs, LCC cells were invariably found within alveolar walls (Figure 1G). In the brain and other organs, LCC cells were closely associated with the vasculature (Figure 1D). Aggressive brain metastatic cells rapidly spread over the abluminal surface of cerebral microcapillaries and this spreading is required for colony outgrowth (Valiente et al., 2014). In contrast, LCC cells infiltrating the brain parenchyma spread along capillaries only transiently (days 1–3 after inoculation) and subsequently adopted a rounded morphology (Figures 1H and 1I).

LCC Cells Are Prone to Enter Quiescence

To monitor proliferation in the first days after inoculation, we labeled LCC cells with 5-ethynyl-2′-deoxyuridine (EdU) prior to intravenous injection into athymic mice (Figures 2A and S2A). Proliferation would dilute the amount of EdU retained in these cells. After 14 days, ~60% of LCC cells that reached the lungs still retained EdU versus 15%–25% in the parental populations (Figures 2B and 2C), indicating that LCC cells entered quiescence more readily. Three months after inoculation, ~90% of H2087-LCC1 cells in lung and HCC1954-LCC1 cells in brain were negative for the proliferation marker Ki-67. Ki-67$^+$ LCC cells were largely confined to cell clusters (Figures 2D and 2E).

To determine the effect of a mitogen-poor environment, we cultured LCC cells in mitogen-low media (MLM, 2% serum) or regular mitogen-rich media (MRM, 10% serum). Under MLM conditions, LCC cells underwent a rapid decrease in proliferation, as determined by their ability to retain EdU in culture (Figure 2F), dye retention (Figure 2G), and CellTiter-Glo assays (Figure S2B), whereas the parental line showed little (H2087) or no decrease (HCC1954) in proliferation. LCC cells accumulated with a G0/G1 DNA content (Figure 2H) and no change in apoptosis marker (cleaved caspase-3) levels (Figure S2C). We performed genome-wide RNA sequencing (RNA-seq) transcriptomic profiling under MRM and MLM conditions. Analysis of differentially expressed genes (Figure S2D) using signatures for specific cell-cycle stages (Croft et al., 2014) showed increased expression of G0/G1-associated genes and lower expression of S phase-associated genes in LCC cells under MLM conditions (Figure S2E).

In sum, LCC cells recapitulated key features of the latent metastatic state, including a propensity to enter proliferative quiescence, an ability to survive as latent entities in relevant organs for months, and a capacity to retain tumorigenic and metastasis-initiating potential. Although LCC cells suffered extensive clearing upon infiltrating target organs, as did the parental population from which they were derived, LCC cells were superior at seeding these organs with a minority of survivors to establish latent metastasis.

LCC Cells Molecularly Cluster with Stem/Progenitor Cells

Gene set enrichment analysis of differentially expressed genes in HCC1954-LCC cells versus parental HCC1954 identified a

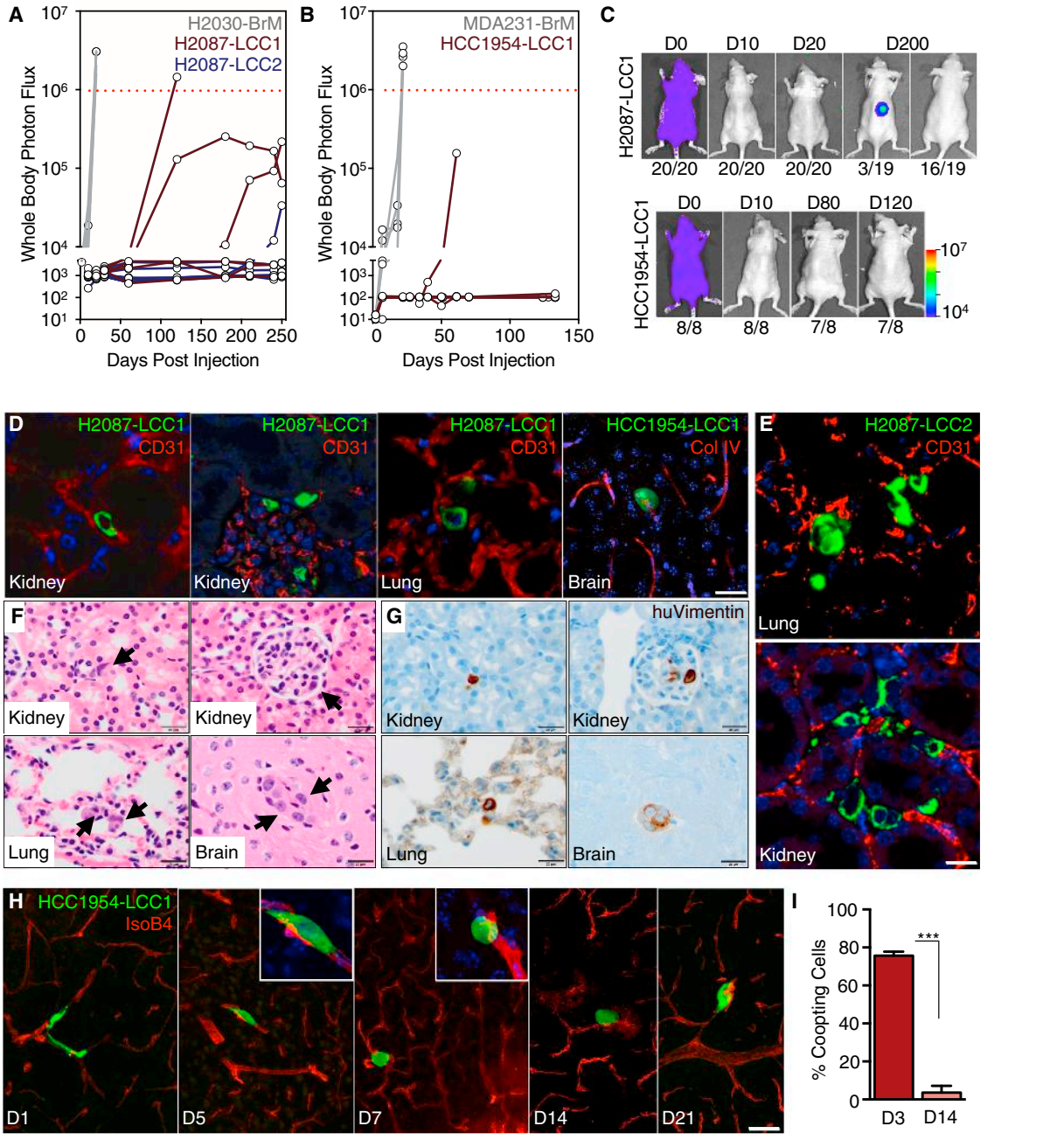

Figure 1. Localization and Dormancy of Disseminated LCC Cells

(A and B) Bioluminescence imaging (BLI) tracking of mice injected with the indicated cell lines. Each line represents an individual mouse. Mice with BLI signal above the dotted red line were euthanized.

(C) Representative images of BLI signal in mice injected with the indicated LCC cell lines. The number of mice represented by each image is indicated at the bottom.

(D) Immunofluorescence staining of disseminated LCC cells (green) next to capillaries (red) in the parenchyma of organ sites. Scale bar, 10 μm.

(E) Infrequent H2087-LCC2 cell (green) clusters in the lung (top panel) or kidney (bottom panel); vasculature (red). Scale bar, 100 μm.

(F) Localization of H2087-LCC1 cells (arrows) in the renal tubule (top-left) or glomeruli (top-right) of the kidney, within alveolar walls of the lung (bottom-left), or capillaries in the brain (bottom-right) 3 months post-injection by H&E staining. Scale bar, 20 μm.

(G) Immunohistochemical staining of disseminated H2087-LCC1 cells from panel 1F with human vimentin (brown). Scale bar, 20 μm.

(H) Time course analysis of HCC1954-LCC1 cell morphology (green) along capillaries (red) as they extravasate and colonize the brain. Scale bar, 50 μm.

(I) Quantification of HCC1954-LCC1 cell morphology in the brain 3 days and 14 days post-injection. Data are mean percentage of coopting cells per brain ± SEM. n = 3 mice per group, scoring representative serial sections of the entire brain for each mouse. ***$p < 0.001$, Student's t test.

See also Figure S1.

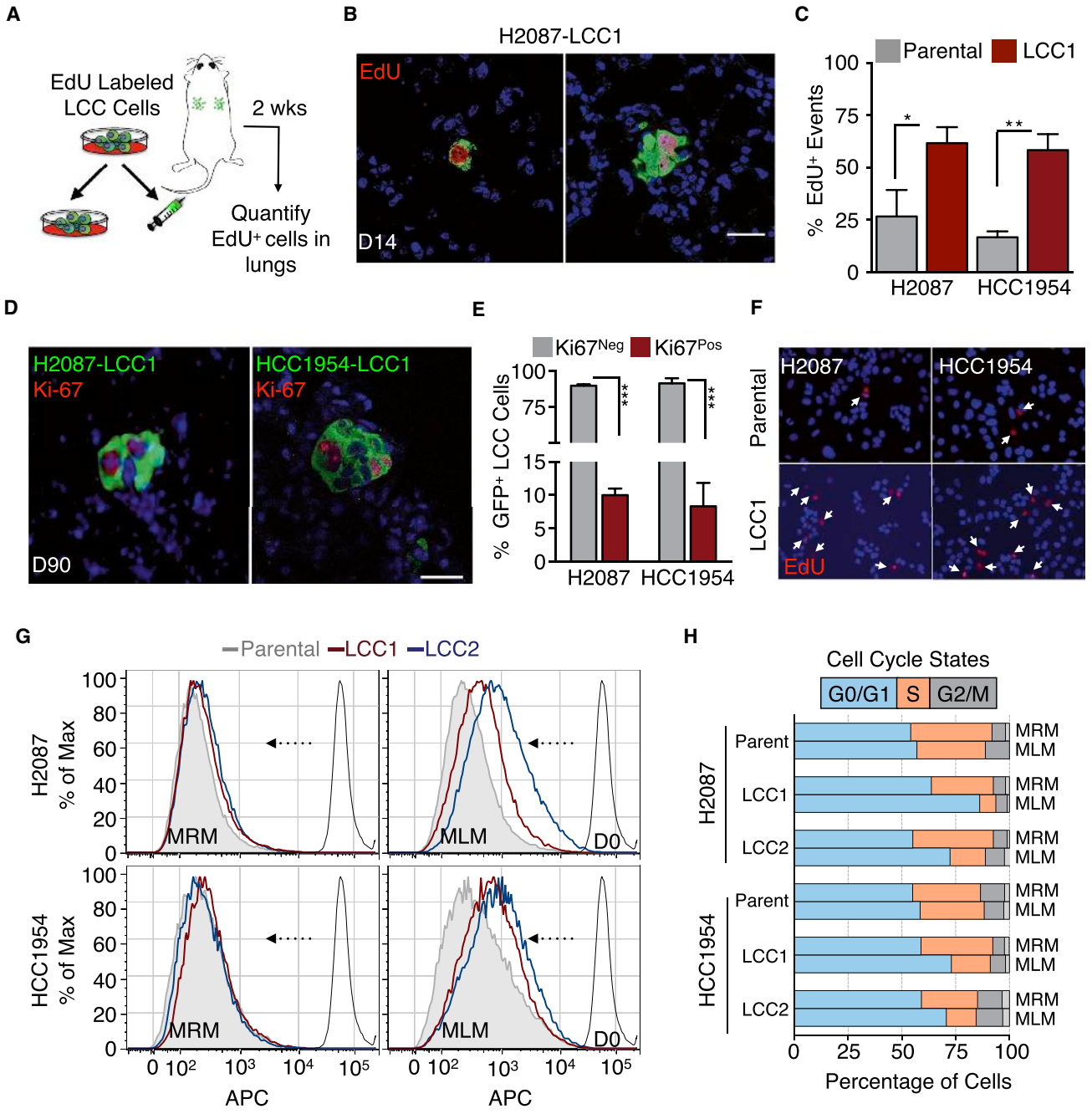

Figure 2. LCC Cells Adopt a Slow-Cycling State In Vitro and In Vivo

(A) Experimental design for EdU pulse-chase experiment.

(B) Immunofluorescence images of double-positive GFP$^+$/EdU$^+$ LCC cells (green, red) in lungs. Scale bar, 10 μm.

(C) Quantification of double-positive EdU$^+$/GFP$^+$ LCC cells versus parental counterparts in lungs harvested 2 weeks post-injection. Data are mean percentage of EdU$^+$ cells per lung ± SEM. n = 3 mice per group, scoring representative serial sections of the entire lung for each mouse. *p < 0.05, **p < 0.01, Mann-Whitney Test.

(D) Representative immunofluorescence images of proliferating Ki-67$^+$ (red) H2087-LCC1 (in lung) and HCC1954-LCC1 cells (in brain) 3 months post-injection. Scale bar, 10 μm.

(E) Quantification of LCC cells from Figure 2D. Data are percentage of total cells that are Ki67$^+$ per organ ± SEM. n = 5 per group, scoring representative serial sections of the entire organ of each mouse. ***p < 0.001, Student's t test. Scale bar, 15 μm.

(F) Micrographs of the indicated cell lines in culture 4 days post EdU labeling. White arrows point to cells retaining EdU label.

(G) Retention of eFluor670 dye by indicated cell lines after 6 days in MRM or MLM culture conditions.

(H) Cell-cycle analysis of the indicated cell lines by BrdU/APC after 3 days in MRM or MLM culture conditions.

See also Figure S2.

mammary stem cell signature (MaSC) as a top-scoring gene set, under both MLM and MRM conditions (Figure S3A). Principal component analysis revealed clustering of HCC1954-LCC cells with human and mouse mammary stem and progenitor cells, away from mature luminal and stromal compartments (Figure 3A) (Lim et al., 2010). Moreover, HCC1954-LCC cells were enriched for the surface marker profile $CD44^{Hi}/CD24^{Lo}$, which is typical of human breast cancer stem cells (Figure 3B) (Al-Hajj et al., 2003).

Based on gene signatures of distinct cell types in the lung epithelium (Treutlein et al., 2014), H2087-LCC cells clustered with the stem-like alveolar type I and bipotent progenitor (BP) cells. Parental H2087 clustered with alveolar type II and Clara cell lineages under MRM and MLM conditions, respectively (Figure 3C). In limiting dilution assays, LCC cells showed a 4- to 15-fold higher probability of engrafting mice compared to parental cells (Figure S3B). These results suggested that our LCC isolation protocol enriched for cancer cells with stem/progenitor cell features.

Sox2 and Sox9 Association with the LCC Phenotype

Progenitor cell identity is determined by lineage-specific transcription factors. Notably, two master regulators of stem and progenitor cell identity, *SOX2* (Arnold et al., 2011) and *SOX9* (Guo et al., 2012), ranked high among transcription factors whose expression was prominently associated with the LCC phenotype. SOX2 was predominant in H2087-LCC cells whereas HCC1954-LCC cells showed high SOX9 expression and low SOX2 expression, both at the mRNA (Figures 3D, S3C, and S3D) and the protein levels (Figure 3E). *SOX2* and *SOX9* regulate stem and progenitor cells in adult tissues (Sarkar and Hochedlinger, 2013). *SOX2* is genetically amplified in squamous carcinomas and small cell lung cancers (Bass et al., 2009; Rudin et al., 2012). *SOX9* is upregulated in brain tumors and basal cell carcinomas (Kordes and Hagel, 2006) and confers stem cell phenotype to breast cancer cells (Guo et al., 2012).

Histone H3 lysine 27 acetylation (H3K27ac) is a mark of transcriptionally active loci (Heintzman et al., 2009). Genome-wide analysis of H3K27ac marks by chromatin immunoprecipitation sequencing (ChIP-seq) revealed distinct patterns in LCC cells compared to the parental counterparts, with 11.9% and 15.6% of the H3K27ac peaks in LCC cells being absent in the H2087 and HCC1954 parental cell populations, respectively, and 7.1% and 24.0% of the H3K27ac peaks in parental cells being absent in the LCC cell populations, respectively (Figure S3E). Enrichment for H3K27ac and Pol II peaks was observed within the *Sox2* locus in H2087 LCC cells (Figure 3F). Although H3K27ac and RNA polymerase II (Pol II) peaks on *SOX9* were observed in HCC1954 LCC cells, we found no difference compared to parental populations (Figure 3G), suggesting that *SOX9* mRNA upregulation in these cells occurs at a post-transcriptional level.

We confirmed expression of SOX2 and SOX9 in LCC cells by immunofluorescence staining in vivo (Figures 3H and 3I). Sox expression was detected in single disseminated LCC cells and in rare proliferating clusters. LCC lesions that grew large accumulated cells with varying levels of Sox2 or Sox9 (see Figure S4A). Related, $CD44^{Hi}/CD24^{Lo}$ mammary cell populations progressively drift toward a higher CD24 content as they divide (Liu et al., 2014). In agreement, sorting HCC1954-LCC2 for cells with a very low CD24 level enriched for Sox9 (Figure S3F).

Metastatic Seeding by LCC Cells Requires Sox Factors

We transduced H2087-LCC and HCC1954-LCC cells with short hairpin RNAs (shRNAs) targeting *SOX2* and *SOX9*, respectively (Figures S3G and S3H). The knockdown inhibited anchorage-independent growth of these cells in Matrigel culture conditions as compared to controls (Figures S3I and S3J). We inoculated these LCC cells into athymic mice by tail vein injection and monitored colonization of the lungs by whole-body BLI imaging weekly for 60 days. Histologic analysis of the lungs showed a marked decrease in the metastatic seeding capacity of the Sox-depleted cells compared to cells expressing a control vector (Figures 3J and 3K).

The ability of tumor-initiating cells to form colonies in suspension provides a test of their capacity to initiate tumor growth (Dontu et al., 2003). LCC cells formed the same number of oncospheres as their parental counterparts (Figure S3K), although LCC oncospheres were smaller (Figure S3L). Interestingly, *SOX2* expression was enriched in H2087-LCC oncospheres, but not oncospheres formed by parental H2087 (Figure S3M). Knockdown of *SOX2* or *SOX9* inhibited oncosphere formation in LCC cells but not in their parental lines (Figures 3L and S3N). We concluded that LCC cells are distinct subpopulations of stem-like cancer cells characterized by high expression of SOX2 or SOX9 and a dependence on these transcription factors for growth under restrictive conditions in vitro and seeding of latent metastasis in mice.

Metastatic Latency Balanced by NK Cell Immune Surveillance

Although LCC cells were superior at seeding organs with latent disease, they still suffered massive attrition in athymic mice. The elimination of disseminated cancer cells may be due to metabolic and mechanical stresses (Goss and Chambers, 2010; Sosa et al., 2014), but also to immune surveillance (Dunn et al., 2004). $FOXN1^{nu}$ athymic mice retain functional NK cells and other components of the innate immune system, raising the possibility that immune surveillance restricts the expansion of LCC cells in these mice. To test this possibility, we inoculated LCC cells into NOD.Cg-$Prkdc^{scid}$ $Il2rg^{tm1Wjl}$/SzJ mice (NOD/SCID Gamma, NSG mice), which are defective for both adaptive and innate immune responses (Shultz et al., 2005). Strikingly, H2087-LCC and HCC1954-LCC cells formed overt metastasis with high penetrance (Figures 4A and 4B) in multiple organs (Figures 4C and 4D). These organs included the liver, a site normally rich in NK cells (Sojka et al., 2014). As the metastatic colonies expanded they accumulated cancer cells with varying levels of SOX2 and SOX9 (Figure S4A).

To test NK cells as candidate inhibitors of LCC expansion, we depleted athymic mice of NK cells by administration of polyclonal anti-asialo-GM1 antibody or anti-NK1.1 monoclonal antibody PK136 (Kasai et al., 1981; Sun and Lanier, 2008) (Figure S4B). Both NK cell depletion strategies resulted in permissive outgrowth of HCC1954-LCC1 cells, as shown by a marked increase in whole-body BLI signal, and an increased metastatic burden in the brain (Figures 4E, 4F, and S4C).

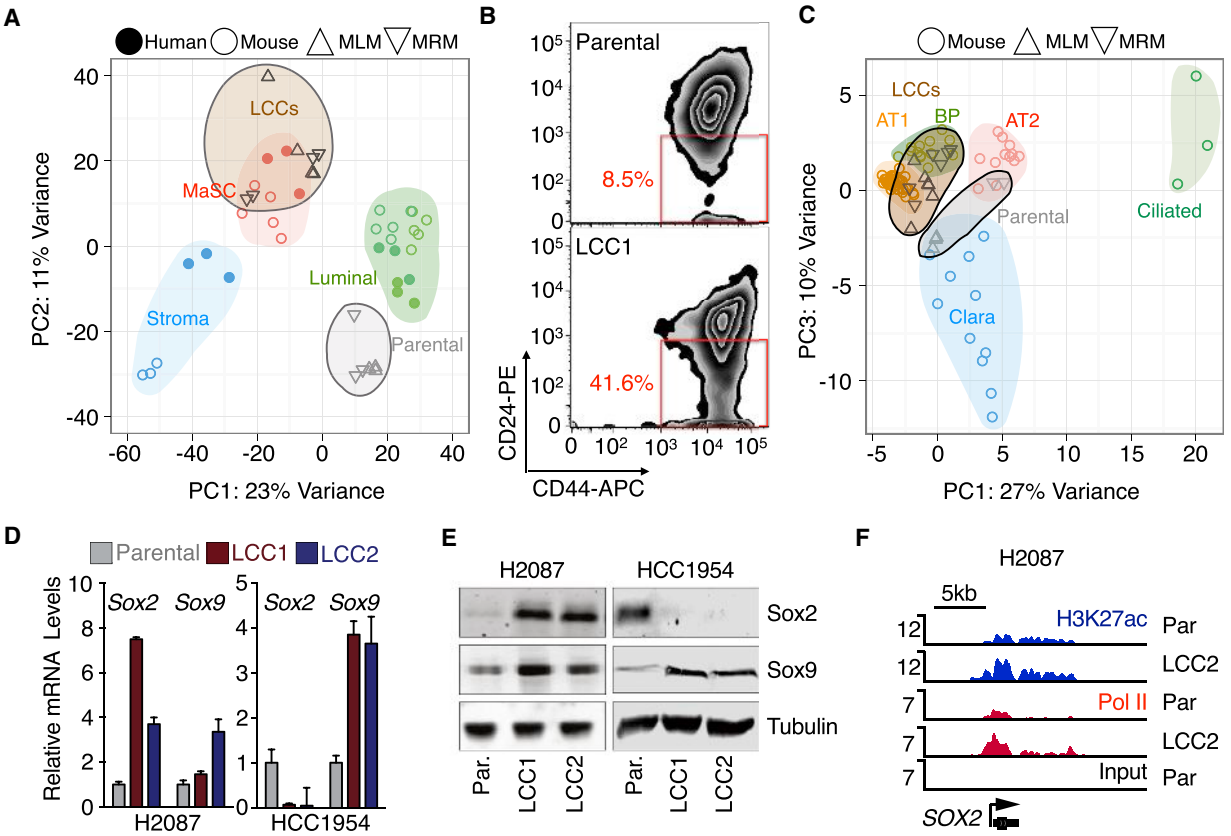

(legend on next page)

Similarly, NK cell depletion increased bone metastasis by H2087-LCC2 (Figure 4G).

To investigate the role of NK cells in immunocompetent mouse models, we used lung adenocarcinoma cell lines derived from tumor-bearing *KRAS*^{G12D}/p53^{Del} mice (Winslow et al., 2011). The 482T1 (T-Met) cell line readily metastasizes to the liver when injected into the spleen of syngeneic B6129SF1 mice, whereas the 368T1 (T-nonMet) line does not. NK cell depletion with anti-asialo-GM1 antibody resulted in a 100-fold increase in the liver metastatic activity of T-nonMet cells, reaching a level that was comparable to that of T-Met cells (Figures S4D and S4E). In a second model, we used 4T07 cells, a non-metastatic cell line derived from a spontaneous BALB/c mouse mammary tumor (Aslakson and Miller, 1992). NK cell depletion of recipient BALB/c mice significantly increased the overall metastatic activity of 4T07 (Figure S4F). Notably, treatment of athymic mice with anti-asialo-GM1 antibody 40 days after inoculation of H2087-LCC or HCC1954-LCC cells triggered an increase in metastatic burden in bones, lungs, and brain compared to controls (Figures 4H–4J).

These results demonstrated the ability of latent LCC cells to stochastically initiate outgrowth when NK cell surveillance in lifted. Collectively, the evidence suggests that LCC cells can proliferate after infiltrating distant organs, but NK cell immune surveillance prevents the accumulation of progeny, sparing LCC cells that entered quiescence. Latent LCC cells remain competent to initiate metastatic outgrowth and abruptly manifest this competence if NK cell surveillance ends.

Downregulation of NK Cell Activators in Quiescent LCC Cells

A balance of activating and inhibitory signals regulates the ability of NK cells to target cancer cells (Vesely et al., 2011; Wu and Lanier, 2003). Oncogenic transformation leads to loss of NK cell inhibitory receptors and upregulation of NK cell activating ligands. During tumor progression, cancer cells evolve to escape NK-cell-mediated recognition (Dunn et al., 2004; Ljunggren and Malmberg, 2007; O'Sullivan et al., 2012). As LCC cells survived NK cell surveillance in athymic mice, we queried LCC gene expression profiles for potential mechanisms of immune evasion. We examined gene expression signatures associated with immune recognition by macrophages, T, B, or NK cells. The expression of NK cytotoxicity signatures was specifically decreased in LCC cells relative to parental cells (Figures S5A and S5B). Moreover, quiescence (MLM) conditions induced further changes in the expression of NK cell ligands in LCC cells (Figures S5C and S5D). The specific genes (Figures 5A and 5B) include several mediators of anti-tumor responses: UL16-binding proteins (ULBP; also known as retinoic acid early transcript, RAET) ULBP2/RAET1H, ULBP3/RAET1N, and ULBP5/RAET1G, which bind to the NK activating receptor NKG2D/CD314 (Lanier, 2015), and PVR/CD155, a ligand for the cancer cell killing NK cell receptor CD226/DNAM-1 (DNAX accessory molecule-1) (Martinet and Smyth, 2015). The pro-apoptotic cytokine receptors FAS and TRAILR, which are critical for NK-cell-mediated target killing (Bradley et al., 1998; Takeda et al., 2001), were also downregulated in LCC cells under quiescence conditions (Figures 5A and 5B). We confirmed the downregulation of CD155 and ULBPs by flow cytometry analysis (Figures 5C, 5D, S5E, and S5F).

To determine whether LCC cells entering quiescence are intrinsically resistant to the cytotoxic action of NK cells, we incubated parental and LCC cells in low-mitogen media and then added freshly isolated, IL-2-activated mouse spleen NK cells to the cultures (Figure 5E). Compared to parental populations, LCC cells showed resistance to cytolysis when incubated with NK cells (Figure 5F). Thus, LCC cells that enter quiescence undergo a striking downregulation of NK cell activators and acquire resistance to NK-cell-mediated killing.

Attenuated WNT Signaling Is Associated with LCC Quiescence

To identify what primes LCC cells to enter this immune evasive quiescent state, we applied signaling pathway classifier analysis to the transcriptomic datasets (Zhang et al., 2009). Under quiescence conditions, H2087-LCC cell isolates showed a reduction in WNT, MYC, and NF-kB signaling, and an increase in TGF-β signaling (Figure 6A). WNT signaling was also attenuated in HCC1954 LCC cells under these conditions (Figure S6A). WNT signaling upregulates MYC (He et al., 1998), and TGF-β causes *MYC* downregulation (Massagué, 2012). A high ratio of phospho-p38 to phospho-ERK kinases, previously described in dormant cancer cell models (Sosa et al., 2014), was present in HCC1954-LCC but not in H2087-LCC cells (Figure S6B).

The drop in WNT signaling in LCC cells that entered quiescence was intriguing. WNT is a potent mitogen for stem and progenitor cells and is implicated in the metastatic outgrowth of lung

Figure 3. LCC Cells Are Enriched for Stem-Cell-like Characteristics

(A) Principal component analysis (PCA) of HCC1954 derivatives and normal breast cell populations of human or mouse origin. HCC1954-LCC cells resemble mammary stem cell (MaSC) gene expression profiles.

(B) Flow cytometry analysis of shows marked enrichment in the CD44^{Hi}/CD24^{Lo} compartment, indicative of breast cancer stem cells in HCC1954 LCC1 cells.

(C) PCA plot of H2087 derivatives and mouse bronchiolar and alveolar cell lineages. H2087-LCC cells cluster with the stem-like alveolar type 1 (AT) and bipotent progenitor (BP) cells.

(D and E) *SOX2* and *SOX9* mRNA (D) and protein (E) expression in the indicated cell lines.

(F and G) Gene track view for H3K27ac and Pol II ChIP-seq data at the *SOX2* locus (F) and *SOX9* locus (G) in the indicated cell lines.

(H and I) Representative single cell and cell cluster images of SOX2- and SOX9-positive H2087-LCC1 in lung and HCC1954-LCC1 in brain. Scale bars, 50 μm.

(J and K) *SOX2* or *SOX9* depletion attenuates survival of H2087-LCC and HCC1954-LCC cells in lungs and brain of athymic mice respectively. Data are total number of LCC cells scored in the lung 3 months post-injection or brains 2 months post injection. n = 5–6 mice per group, scoring representative serial sections of the organ. ***$p < 0.001$, Mann-Whitney test.

(L) Oncosphere-forming capacity upon *SOX2* and *SOX9* depletion in the indicated cell lines. Each panel depicts representative control or SOX2/SOX9-depleted cell oncospheres. **$p < 0.01$, ***$p < 0.001$, Student's t test.

See also Figure S3.

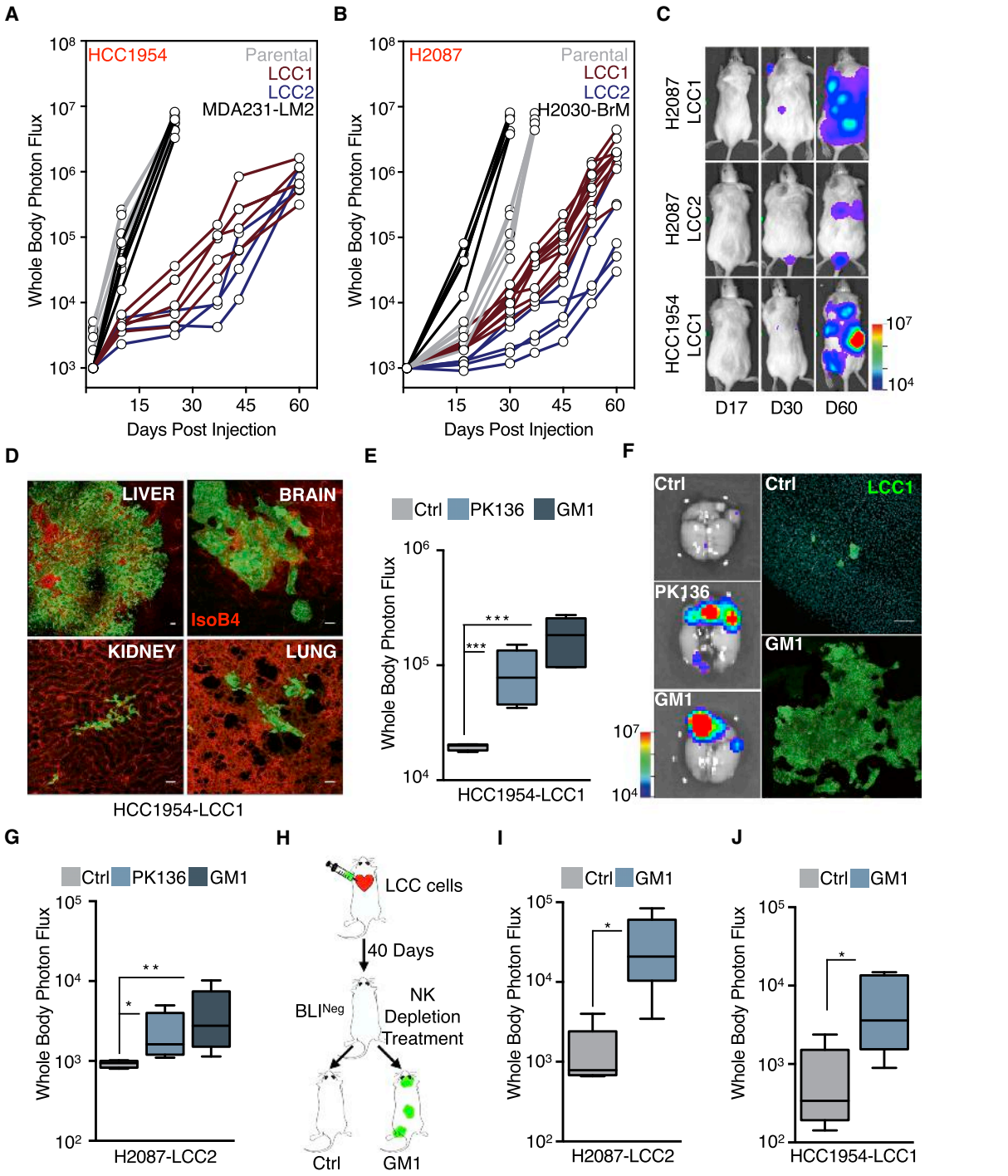

Figure 4. LCC Cells Are in Equilibrium with the Innate Immune System

(A and B) BLI tracking of NSG mice injected with the indicated cell lines. Each line represents one mouse.

(C) Representative images of BLI signal in NSG mice injected with the indicated LCC cell lines over the indicated time period.

(D) Metastatic outgrowth of HCC1954-LCC1 (green) in the liver, brain, kidney, and lungs of NSG mice 2 months post-injection. Vasculature, isolectin-B4 (red). Scale bar, 100 μm.

(E and F) Depletion of NK cells by either anti-NK1.1 (PK136) or anti-asialo-GM1 antibody regimen allows outgrowth of HCC1954-LCC1 cells injected in athymic nude mice. Outgrowth quantified by whole body photon flux at 2 months post-injection, with whisker plots representing minimum and maximum values. n = 5–7 mice per group. ***$p < 0.001$, Mann-Whitney test. Representative ex vivo brain BLI images of mice and brain tissue sections show massive outgrowth of HCC1954-LCC1 cells (green) upon NK depletion (F). Scale bar, 100 μm.

(legend continued on next page)

adenocarcinoma (Nguyen et al., 2009) and breast cancer stem cells (Malanchi et al., 2012; Oskarsson et al., 2011). H2087-LCC cells in MLM conditions showed resistance to pathway activation by WNT3A addition, as determined by *AXIN2* expression (Figure 6B) and TCF transcriptional reporter activation (Figure S6C) (Fuerer and Nusse, 2010). We assessed WNT activity in LCC cells in vivo by immunostaining for active β-catenin, a marker for canonical WNT pathway activation. We detected higher levels of active β-catenin in proliferating LCC cell clusters than in single disseminated LCC cells in the brain (Figure 6C). Thus, LCC cells have a propensity to resist WNT pathway activation.

Autocrine DKK1 Expression in LCC Cells

These results raised the possibility that LCC cells entering quiescence express a WNT inhibitor. Indeed, we observed that the WNT inhibitor dickkopf-related protein 1 (DKK1) was highly expressed in LCC cell lines (Figures 6D and S6D). ChIP-seq analysis showed a clear increase in H3K27ac and Pol II peaks at the *DKK1* locus in both LCC models, compared to the parental lines (Figures 6E and 6F). Immunofluorescence staining demonstrated DKK1 expression in LCC cells in vivo (Figure 6G).

We extended these results with breast cancer patient-derived xenografts (PDXs). Surgical orthotopic implantation of the hormone receptor-negative PDX models HCI-001 and HCI-002, and the HER2$^+$ PDX model HCI-008 gives rise to tumors with no visible metastasis (DeRose et al., 2011). PDX tumors expressed human vimentin, which we used as a surrogate marker to identify DTCs in the lungs, brain, and kidneys of mice bearing these tumors. A total of 14%–51% of disseminated cancer cells were positive for both human vimentin and DKK1 (Figures S6E and S6F), demonstrating an association of DKK1 with DTCs from orthotopically implanted PDX models.

DKK1 is a direct transcriptional target of Sox2 in mesenchymal stem cells, with Sox2 binding 75 bp upstream of the transcriptional start site (Park et al., 2012; Seo et al., 2013). Indeed, H2087-LCC1 cells showed *SOX2* binding to this promoter region (Figure 6H). Stable shRNA knockdown of *SOX2* in LCC cells decreased the expression of DKK1 (Figure 6I). DKK1 knockdown (Figures S6G and S6H) re-sensitized LCC cells to WNT pathway activation (Figure 6J). CellTiter-Glo assays and dye retention assays (Figures 6K and S6I) showed that DKK1 knockdown stimulated the proliferation of LCC cells under low-mitogen conditions. In complementary experiments, incubation of parental H2087 cells with recombinant DKK1 inhibited WNT3A response and proliferation in LCC cells (Figures 6L and S6J).

Autocrine DKK1 Enforces a Quiescent, Immune Evasive State in Latent Metastasis

The preceding results suggested that autocrine DKK1 primes LCC cells to enter quiescence, which leads to downregulation of NK cell activators. One prediction of this model is that autocrine DKK1 is required to protect LCC cells from elimination in athymic mice. In line with this prediction, shRNA-mediated DKK1 depletion in H2087-LCC cells significantly decreased the accumulation of LCC cells in the lungs of inoculated athymic mice (Figure 7A). Ki-67$^+$ stromal cells surrounded the cancer cells in bronchiolar regions under these conditions. Many of these stromal cells were positive for the leukocyte common antigen CD45 and included Ly6B.2$^+$ neutrophils and F4/80$^+$ inflammatory monocytes and macrophages, suggesting that LCC cell proliferation triggers lymphocyte infiltration for cancer cell clearance (Figures S7A and S7B). DKK1 knockdown in H2087-LCC cells increased the expression of NK cell activating ligands ULBP1, ULBP2, ULBP4, and ULBP5 and death signal receptors (Figure 7B). Conversely, addition of a high concentration of WNT3A to H2087-LCC1 cells increased the expression of ULBP1 and ICAM1 (Figure S7B). DKK1-depleted cells were more susceptible to NK-cell-mediated cytotoxicity (Figure 7C). Moreover, depletion of NK cells in athymic mice rescued the formation of macrometastases by DKK1-knockdown H2087-LCC cells (Figures 7D and S7C).

In contrast to the deleterious effect of DKK1 knockdown on the viability of LCC cells in athymic mice, DKK1 knockdown increased the metastatic growth of H2087 and HCC1954 LCC cells in NSG mice (Figures 7E, 7F, and S7D). Conversely, overexpressing DKK1 in H2087-parental cells decelerated their growth in NSG mice (Figures S7E and S7F). As a corollary, depletion of SOX2 in H2087-LCC or SOX9 in HCC1954-LCC cells inhibited the ability of these cells to form metastasis in NSG mice (Figures 7G and S7G). No significant effect was observed upon SOX2 and SOX9 depletion in parental populations (Figure S7H). These data confirmed the essential role of SOX transcription factors for metastatic growth of LCC cells in the presence or absence of NK cells and the ability of NK cells to restrain LCC outgrowth but spare LCC cells that enter quiescence.

DISCUSSION

Our results show that cancer cell populations selected from lung and breast cancer cell lines for their competence to establish latent metastasis have high expression of stem/progenitor markers. They also have a capacity to enter immune evasive quiescence while retaining metastasis-initiating powers. These cells, which we operationally call latency competent cancer cells, suffer extensive attrition upon infiltrating target organs, as their unselected parental populations do. However, LCC cells can stochastically enter a self-imposed quiescent state, which leads to downregulation of NK cell ligands for evasion of immune surveillance. NK cells kill dividing LCC cells but spare quiescent LCC cells. As a result, cancer cells in these models can persist long-term as latent metastasis seeds in different organs (Figure 7H).

(G) NK cell depletion regimens also allow for outgrowth of H2087-LCC2 cells in athymic nude mice. Whole body photon flux at 2 months post-injection, with whisker plots representing minimum and maximum values. n = 5–7 mice per group. *p < 0.05, **p < 0.01, Mann-Whitney test.
(H) NK depletion scheme in mice injected with LCC cells.
(I and J) NK cell depletion regimen 40 days post extravasation allows for outgrowth of the indicated cell lines in athymic nude mice. Outgrowth quantified by whole body photon flux, with whisker plots representing minimum and maximum values. n = 5 mice per group. *p < 0.05. Mann-Whitney test.
See also Figure S4.

A

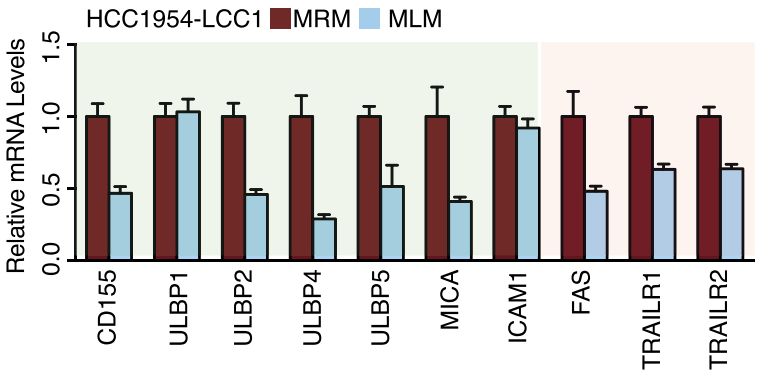

B

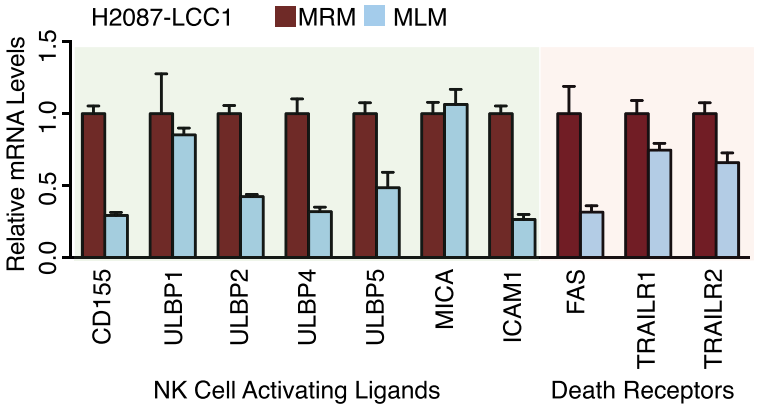

C

Cell lines	% CD155 Pos.	
	MRM	MLM
H2087-Par.	60.5	45.3
H2087-LCC1	45.3	**14.0**
HCC1954-Par.	41.0	38.2
HCC1954-LCC1	25.0	**11.3**

D

Cell lines	% ULBP2/5/6 Pos.	
	MRM	MLM
H2087-Par.	22.8	16.7
H2087-LCC1	17.8	**4.2**
HCC1954-Par.	20.5	16.0
HCC1954-LCC1	10.0	**4.8**

E

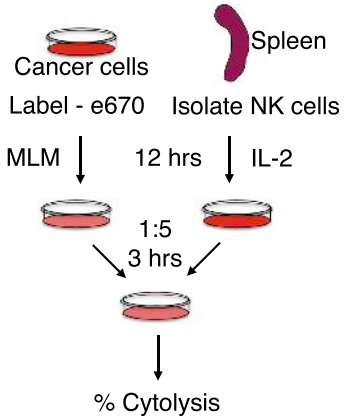

F

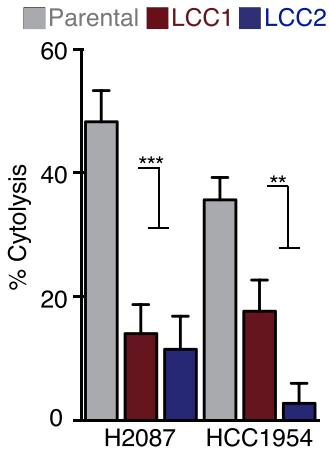

Figure 5. LCC Cells Evade NK-Cell-Mediated Immune Surveillance

(A and B) Genes important for NK cell recognition and cytotoxicity are downregulated in the indicated cell lines when grown in MLM conditions.

(C and D) Cell surface expression of NK cell activating ligands CD155 and ULBP 2/5/6 in the indicated cell lines under MRM and MLM culture conditions.

(E) Schematic of in vitro NK cell cytotoxicity experiment. Labeled cancer cells were incubated with activated primary NK cells at a 1:5 target:effector ratio for 3 hr, followed by quantification of remaining intact cancer cells.

(F) H2087 and HCC1954-LCC cells are more resistant to NK-cell-mediated cytotoxicity compared to parental counterparts. Data are mean percentage of cytolysis ± SEM for three replicates. $^{**}p < 0.01$, $^{***}p < 0.001$, Student's t test.

See also Figure S5.

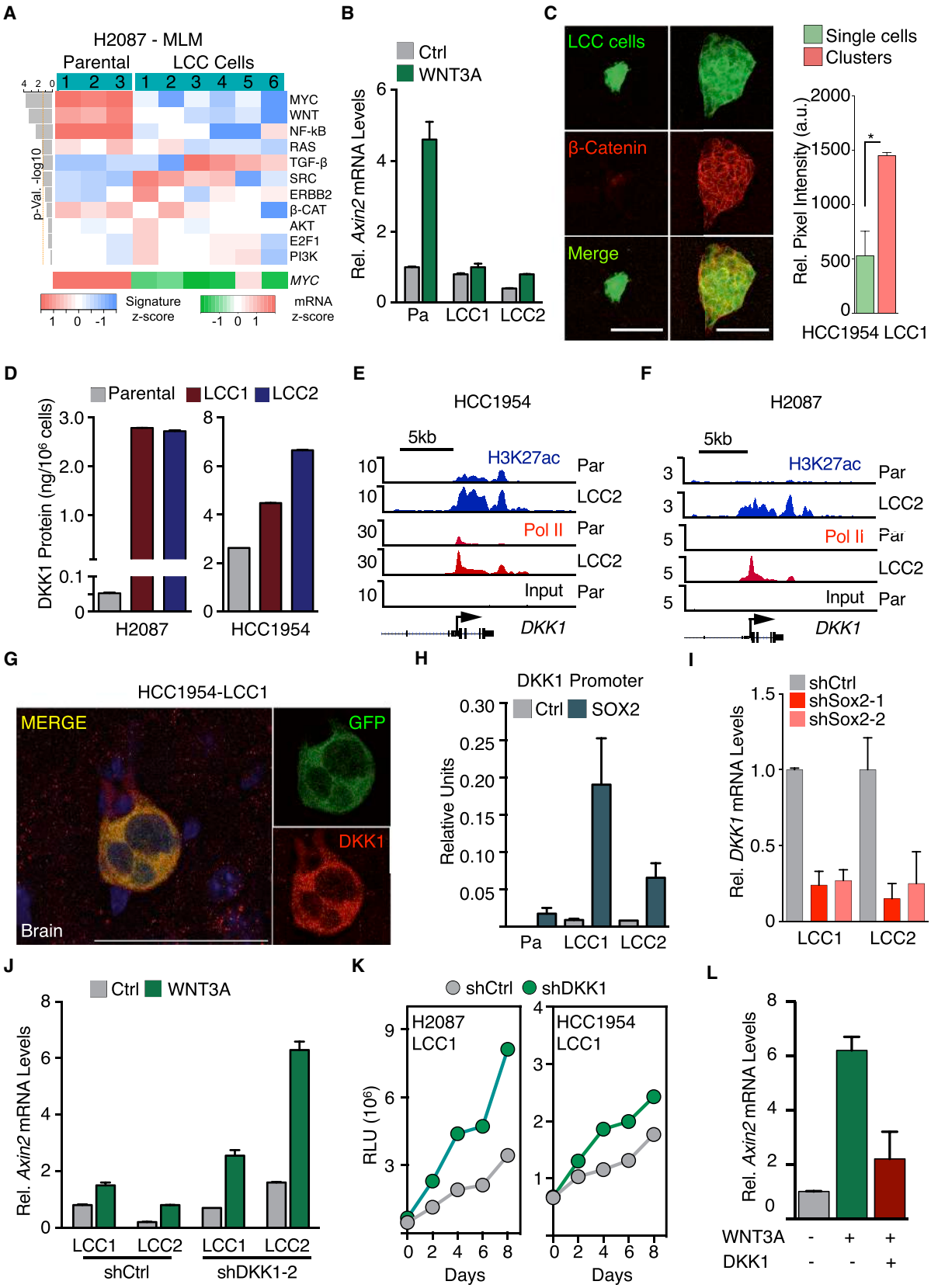

(legend on next page)

Stem-like Nature of Latency Competent Cancer Cells

A defining trait of LCC cells is their stem-like phenotype. At the molecular level, breast cancer and lung cancer LCC cells resemble mammary stem cells or lung alveolar bi-potent progenitors, respectively. LCC cells express *SOX2* or *SOX9*, transcription factors that play critical roles in stem cell identity and pluripotency. *SOX2* and *SOX9* enforce stemness in lung and breast adenocarcinomas, respectively (Arnold et al., 2011; Guo et al., 2012). We show that expression of *SOX2* and *SOX9* is essential for the survival and metastasis-initiating properties of LCC cells in multiple host tissues. Adult stem cells can exist in an actively dividing pool for homeostatic tissue renewal and a slow-cycling pool responsible for tissue regeneration upon injury (Li and Clevers, 2010; Lien and Fuchs, 2014). LCC cells may be segmented into these two phenotypes as well. After infiltrating target organs, proliferating LCC cells are eliminated by NK cells. However, by entering quiescence, a minority of LCC cells can evade NK cell surveillance (Figure 7H).

Self-Imposed Quiescence

Growth inhibitory signals from the host microenvironment and the perivascular niche, including TGF-β and BMP, can contribute to metastatic dormancy (Sosa et al., 2014). However, disseminated cancer cells are likely exposed to mitogenic signals during the course of latency periods, as perivascular niches in the host organs support tissue homeostasis and regeneration though stromal WNT and other proliferative signals. Our results demonstrate an innate ability of LCC cells to self-impose a slow cycling state in this context. This ability is based on the expression of the WNT inhibitor DKK1, which prevents activation of β-catenin and LCC cell proliferation. DKK1 is a direct transcriptional target of SOX2 in LCC cells. We show that autocrine DKK1 helps disseminated LCC cells enter quiescence. In the model, this self-imposed quiescence counterbalances the action of stromal WNT signals to preserve the viability of residual LCC cells in the host tissue (Figure 7H).

Quiescence-Associated Immune Evasion

Proliferative quiescence protects LCC cells from NK-mediated killing. On entering, quiescence LCC cells downregulate cell surface ULBP activators of NK-cell-mediated cytotoxicity and receptors for cell death signals. In mice with an active innate immune system, LCC cells are mostly found as quiescent single cells. Rare LCC cell clusters observed under these conditions contain actively proliferating cells, but may be fated to undergo NK-mediated clearance. Depletion of NK cells by different means in different mouse models led to aggressive metastatic outgrowth of LCC cells, arguing that quiescent LCC cells stochastically enter the cell cycle, and the proliferative clusters will progress to macrometastases if immune surveillance is relaxed. The ability to undergo periodic bursts of proliferation and elimination, with a small fraction of the progeny entering quiescence and surviving after each round, would allow disseminated cancer cells to evolve additional metastatic traits, such as active immunosuppression and organ-specific colonization traits, for an eventual macrometastatic outbreak (Figure 7H). Metastatic evolution would be less likely in a permanently quiescent cancer cell population.

Therapeutic Implications

Our observations in latent metastasis are in line with the role of immune surveillance in restricting malignant cell proliferation in other contexts. Clinically, the presence of NK cell infiltrates in primary colorectal, gastric, and lung cancer correlates with better patient survival outcomes, consistent with an ability of NK to keep metastases in check (Jin et al., 2014; Villegas et al., 2002). Because NK cells have the ability to limit LCC cell outgrowth, a drop in NK cytotoxicity index in disease-free cancer patients might serve as a prognostic indicator of disease relapse. The possibility of treating residual disease by inducing proliferation in order to re-sensitize cancer cells to adjuvant cytotoxic chemotherapy would entail the risk of triggering metastasis while trying to prevent it. Our findings raise the possibility of selectively reactivating NK cell ligands in quiescent metastatic cells in order to trigger the immunologic elimination of latent metastasis.

EXPERIMENTAL PROCEDURES

Animal Studies

All animal experiments were done in accordance with the guidelines provided by the MSKCC Institutional Animal Care and Use Committee. Athymic

Figure 6. Attenuated WNT Signaling Enforces Quiescence in LCC Cells

(A) Signaling pathway response signature analysis of H2087 derivatives under MLM conditions shows marked reduction in WNT and MYC pathway activity (upper panel). *MYC* mRNA *Z* score of these derivatives was scored from RNA-seq data (lower panel).

(B) H2087-LCC cells are less responsive to WNT pathway activation by WNT3A stimulation as measured by *AXIN2* expression.

(C) Immunofluorescence images showing active β-catenin expression (red) in clusters compared to HCC1954 LCC single cells in the brain. Quantification of relative pixel intensity of β-catenin is shown. n = 5 representative sections per condition. *$p < 0.05$, Student's t test. Scale bar, 50 μm.

(D) DKK1 protein expression levels (ELISA) in H2087 and HCC1954-LCC derivatives relative to parental. Data are mean amount of secreted DKK1 protein ± SEM. n = 3 technical replicates per group.

(E and F) Gene track view for H3K27ac and Pol II ChIP-seq data at the DKK1 locus in HCC1954 and H2087 parental and LCC cells. DKK1 gene body is represented at the bottom.

(G) HCC1954-LCC1 cells (green) detected in the brain parenchyma 1 month post-injection in athymic nude mice express DKK1 (red). Scale bar, 50 μm.

(H) SOX2 binding to the DKK1 promoter assayed by SOX2 ChIP followed by qRT-PCR analysis of the DKK1 promoter in H2087 derivatives. Error bars ± SD.

(I) *DKK1* mRNA expression is diminished in H2087-LCC cells depleted of *SOX2*.

(J) WNT pathway activation by WNT3a stimulation in H2087-LCC cells depleted of DKK1. Relative mRNA expression of *AXIN2* used as marker for WNT pathway activation.

(K) Tracking of cell proliferation in the indicated cell lines cultured under MLM conditions by CellTiter-Glo assay.

(L) Responsiveness of H2087 parental cells to WNT-signaling induction by WNT3A stimulation in the presence or absence of recombinant human DKK1.

See also Figure S6.

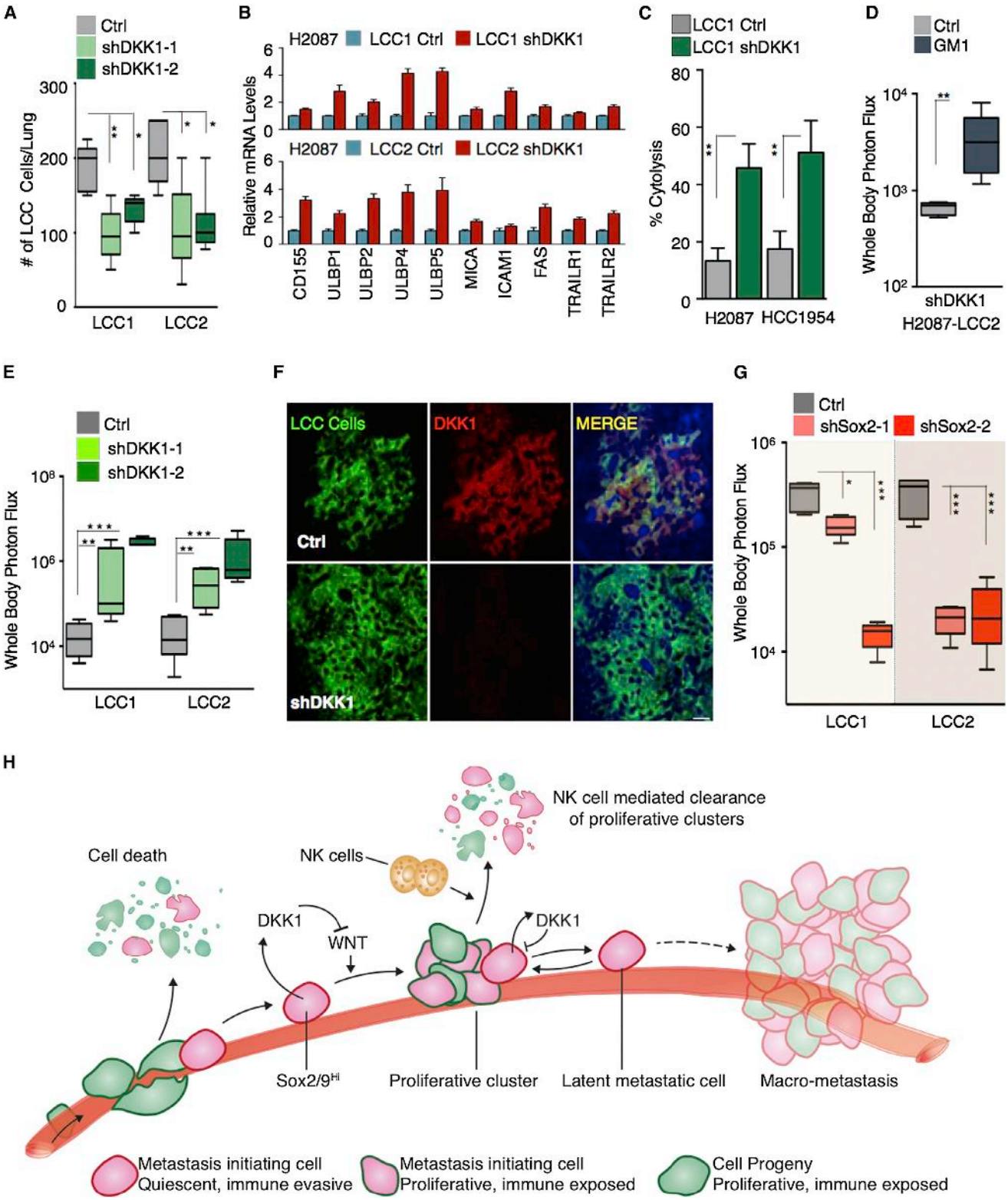

Figure 7. DKK1 Enforces a Quiescent Immune Evasive State

(A) Growth of H2087-LCC cells depleted of DKK1 in athymic nude mice. Data are total number of LCC cells detected per lung after 3 months post-tail vein injection ± SEM. N = 5–6 mice per group, scoring representative serial sections of the entire lung for each mouse.

(legend continued on next page)

(NCI/Charles River/Harlan), BALB/c, B6129SF1, or NOD *SCID gamma* (Jackson Laboratory) female mice from 4-6 weeks of age were used for in vivo studies. For experimental metastasis assays, 1.0 × 10^5 cells were resuspended in 100 μl 1× PBS and intracardially injected into the right ventricle with a 26G tuberculin syringe. Lung colonization assays were performed by injecting 0.5/1.0 × 10^5 cells into the lateral tail vein of mice with a 28G insulin syringe. We detected metastatic burden by non-invasive bioluminescence imaging of experimental animals using an IVIS Spectrum (PerkinElmer). Bioluminescence signal was measured using the ROI tool in Living Image 4.4 software (PerkinElmer).

LCC Isolation and Culture

Cells (1.0 × 10^5) expressing a lentiviral TK-GFP-luciferase (TGL) construct in combination with antibiotic resistance marker Blasticidin (H2087) or Puromycin (HCC1954) in a volume of 100 μl was intracardially injected into the left cardiac ventricle of anesthetized (ketamine 100 mg/kg, xylazine 10 mg/kg) 4- to 6-week-old athymic mice. Cancer cell colonization was tracked by retro-orbital injection of D-luciferin (150 mg/kg) and imaged with an IVIS Spectrum (PerkinElmer). Bioluminescence (BLI) analysis was performed with Living Image 4.4 software.

Organs from BLI-negative mice were resected under sterile conditions and mechanically dissociated using a gentleMACS dissociator (Miltenyl Biotec) and placed in culture medium containing a 1:1 mixture of DMEM/Ham's F12 supplemented with 0.125% collagenase III and 0.1% hyaluronidase. Minced samples were incubated at 37°C for 1 hr, with gentle rocking to produce single cell suspensions. After collagenase treatment, cells were briefly centrifuged, resuspended in 0.25% trypsin, and incubated for a further 15 min at 37°C. Cells were then resuspended in their respective culture conditions and allowed to grow to confluence on a 15-cm dish. Cancer cells from these BLI-negative organs were selected for by adding respective antibiotics to the media.

ACCESSION NUMBERS

The accession number for the raw RNA-seq and ChIP-seq data reported in this paper is GEO: GSE72956.

SUPPLEMENTAL INFORMATION

Supplemental Information includes Supplemental Experimental Procedures and seven figures and can be found with this article online at http://dx.doi.org/10.1016/j.cell.2016.02.025.

AUTHOR CONTRIBUTIONS

S.M. and J.M. conceived the project and designed the experiments. S.M. and D.G.M. performed most experiments. X.J. and L.H. assisted with experiments. E.D. provided assistance with PDX models. H.B. performed ChIP-seq experiments. X.J., D.G.M., and Y.Z. performed computational analysis. S.M., D.G.M., and J.M. wrote the paper. All authors discussed results and revised the manuscript.

ACKNOWLEDGMENTS

We thank P. Bos, T. O'Sullivan, and J. Sun for insightful discussions and advice on NK cell depletion experiments; A. Welm for breast PDX models; S. Monette for review of pathology slides; T. Jacks and F. Giancotti for cell lines; and A. Obenauf, K. Ganesh, A. Laughney, and E. Er for critical reading of the manuscript. We acknowledge the support of the Memorial Sloan Kettering Cancer Center (MSKCC) Genomics Core Facility and Molecular Cytology Core Facility. This work was supported by NIH grants P01-CA094060 and P01-CA129243, and DOD Innovator Award W81XWH-12-1-0074 (J.M.), and NIH grant P30-CA008748 (MSKCC). S.M. is supported by an American Cancer Society post-doctoral fellowship. X.J. is a Susan G. Komen Fellow. H.B. is a Damon Runyon Fellow.

Received: September 17, 2015
Revised: December 21, 2015
Accepted: February 10, 2016
Published: March 24, 2016

REFERENCES

Al-Hajj, M., Wicha, M.S., Benito-Hernandez, A., Morrison, S.J., and Clarke, M.F. (2003). Prospective identification of tumorigenic breast cancer cells. Proc. Natl. Acad. Sci. USA *100*, 3983–3988.

Arnold, K., Sarkar, A., Yram, M.A., Polo, J.M., Bronson, R., Sengupta, S., Seandel, M., Geijsen, N., and Hochedlinger, K. (2011). Sox2(+) adult stem and progenitor cells are important for tissue regeneration and survival of mice. Cell Stem Cell *9*, 317–329.

Aslakson, C.J., and Miller, F.R. (1992). Selective events in the metastatic process defined by analysis of the sequential dissemination of subpopulations of a mouse mammary tumor. Cancer Res. *52*, 1399–1405.

Bass, A.J., Watanabe, H., Mermel, C.H., Yu, S., Perner, S., Verhaak, R.G., Kim, S.Y., Wardwell, L., Tamayo, P., Gat-Viks, I., et al. (2009). SOX2 is an amplified lineage-survival oncogene in lung and esophageal squamous cell carcinomas. Nat. Genet. *41*, 1238–1242.

Bradley, M., Zeytun, A., Rafi-Janajreh, A., Nagarkatti, P.S., and Nagarkatti, M. (1998). Role of spontaneous and interleukin-2-induced natural killer cell activity in the cytotoxicity and rejection of Fas+ and Fas- tumor cells. Blood *92*, 4248–4255.

Bragado, P., Estrada, Y., Parikh, F., Krause, S., Capobianco, C., Farina, H.G., Schewe, D.M., and Aguirre-Ghiso, J.A. (2013). TGF-β2 dictates disseminated

(B) Relative mRNA expression of NK cell activating ligands and death receptors in H2087-LCC cells upon DKK1 depletion. Relative quantification is normalized to LCC1 or LCC2 control.
(C) H2087 and HCC1954-LCC cells depleted of DKK1 are more susceptible to NK-cell-mediated cytotoxicity compared to their controls. Data are mean percentage of cytolysis ± SEM for three replicates. **$p < 0.01$, Student's t test.
(D) Depletion of NK cells by anti-asialo-GM1 in athymic nude mice injected with shDKK1 bearing H2087-LCC2 cells. Whole body photon flux, 2 months post-injection. N = 5–6 mice per group. **$p < 0.01$, Mann-Whitney test.
(E) Growth of H2087-LCC cells depleted of DKK1 in NSG mice. Whole body photon flux, 2 months post-injection. N = 5–6 mice per group. **$p < 0.01$, ***$p < 0.001$, Mann-Whitney test.
(F) Representative immunofluorescence images of metastatic lesions in the lungs of NSG mice in (E). Scale bar, 50 μm.
(G) Growth of H2087-LCC cells depleted of Sox2 in NSG mice. Whole body photon flux, 2 months post-injection. N = 5–6 mice per group. *$p < 0.05$, ***$p < 0.001$, Mann-Whitney test.
(H) A model summarizing the central tenets of latency recapitulated in the present latency competent cancer cell models. A majority of disseminated cancer cells including LCC cells suffer massive attrition in circulation or upon extravasation due to mechanical and metabolic stress and immune surveillance. LCC cells associate with the vasculature, are enriched for Sox2/Sox9 stem-cell-like programs, stochastically enter proliferative quiescence, and are superior at seeding organs. LCC cells can proliferate in response to stimulatory microenvironmental cues after infiltrating distant organs, but NK-cell-dependent immune surveillance prevents accumulation of their progeny, sparing only LCC cells that entered quiescence stochastically. Cells enriched for DKK1 are able to attenuate the proliferative response to local WNT signals, enter quiescence. Quiescent cells downregulate the expression of cell surface NK sensors to evade immune surveillance. Surviving latent metastatic cells may evolve, accumulating traits for eventual outbreak to form macrometastases (refer to Discussion).
See also Figure S7.

tumour cell fate in target organs through TGF-β-RIII and p38α/β signalling. Nat. Cell Biol. *15*, 1351–1361.

Braun, S., Vogl, F.D., Naume, B., Janni, W., Osborne, M.P., Coombes, R.C., Schlimok, G., Diel, I.J., Gerber, B., Gebauer, G., et al. (2005). A pooled analysis of bone marrow micrometastasis in breast cancer. N. Engl. J. Med. *353*, 793–802.

Croft, D., Mundo, A.F., Haw, R., Milacic, M., Weiser, J., Wu, G., Caudy, M., Garapati, P., Gillespie, M., Kamdar, M.R., et al. (2014). The Reactome pathway knowledgebase. Nucleic Acids Res. *42*, D472–D477.

DeRose, Y.S., Wang, G., Lin, Y.C., Bernard, P.S., Buys, S.S., Ebbert, M.T., Factor, R., Matsen, C., Milash, B.A., Nelson, E., et al. (2011). Tumor grafts derived from women with breast cancer authentically reflect tumor pathology, growth, metastasis and disease outcomes. Nat. Med. *17*, 1514–1520.

Dontu, G., Abdallah, W.M., Foley, J.M., Jackson, K.W., Clarke, M.F., Kawamura, M.J., and Wicha, M.S. (2003). In vitro propagation and transcriptional profiling of human mammary stem/progenitor cells. Genes Dev. *17*, 1253–1270.

Duchnowska, R., Dziadziuszko, R., Czartoryska-Arłukowicz, B., Radecka, B., Szostakiewicz, B., Sosińska-Mielcarek, K., Karpińska, A., Starosławska, E., Kubiatowski, T., and Szczylik, C. (2009). Risk factors for brain relapse in HER2-positive metastatic breast cancer patients. Breast Cancer Res. Treat. *117*, 297–303.

Dunn, G.P., Old, L.J., and Schreiber, R.D. (2004). The immunobiology of cancer immunosurveillance and immunoediting. Immunity *21*, 137–148.

Eyles, J., Puaux, A.L., Wang, X., Toh, B., Prakash, C., Hong, M., Tan, T.G., Zheng, L., Ong, L.C., Jin, Y., et al. (2010). Tumor cells disseminate early, but immunosurveillance limits metastatic outgrowth, in a mouse model of melanoma. J. Clin. Invest. *120*, 2030–2039.

Fuerer, C., and Nusse, R. (2010). Lentiviral vectors to probe and manipulate the Wnt signaling pathway. PLoS ONE *5*, e9370.

Gao, H., Chakraborty, G., Lee-Lim, A.P., Mo, Q., Decker, M., Vonica, A., Shen, R., Brogi, E., Brivanlou, A.H., and Giancotti, F.G. (2012). The BMP inhibitor Coco reactivates breast cancer cells at lung metastatic sites. Cell *150*, 764–779.

Gazdar, A.F., and Minna, J.D. (1996). NCI series of cell lines: an historical perspective. J. Cell. Biochem. Suppl. *24*, 1–11.

Gazdar, A.F., Kurvari, V., Virmani, A., Gollahon, L., Sakaguchi, M., Westerfield, M., Kodagoda, D., Stasny, V., Cunningham, H.T., Wistuba, I.I., et al. (1998). Characterization of paired tumor and non-tumor cell lines established from patients with breast cancer. Int. J. Cancer *78*, 766–774.

Goss, P.E., and Chambers, A.F. (2010). Does tumour dormancy offer a therapeutic target? Nat. Rev. Cancer *10*, 871–877.

Guo, W., Keckesova, Z., Donaher, J.L., Shibue, T., Tischler, V., Reinhardt, F., Itzkovitz, S., Noske, A., Zürrer-Härdi, U., Bell, G., et al. (2012). Slug and Sox9 cooperatively determine the mammary stem cell state. Cell *148*, 1015–1028.

He, T.C., Sparks, A.B., Rago, C., Hermeking, H., Zawel, L., da Costa, L.T., Morin, P.J., Vogelstein, B., and Kinzler, K.W. (1998). Identification of c-MYC as a target of the APC pathway. Science *281*, 1509–1512.

Heintzman, N.D., Hon, G.C., Hawkins, R.D., Kheradpour, P., Stark, A., Harp, L.F., Ye, Z., Lee, L.K., Stuart, R.K., Ching, C.W., et al. (2009). Histone modifications at human enhancers reflect global cell-type-specific gene expression. Nature *459*, 108–112.

Jin, S., Deng, Y., Hao, J.W., Li, Y., Liu, B., Yu, Y., Shi, F.D., and Zhou, Q.H. (2014). NK cell phenotypic modulation in lung cancer environment. PLoS ONE *9*, e109976.

Kasai, M., Yoneda, T., Habu, S., Maruyama, Y., Okumura, K., and Tokunaga, T. (1981). In vivo effect of anti-asialo GM1 antibody on natural killer activity. Nature *291*, 334–335.

Kitamura, T., Qian, B.Z., and Pollard, J.W. (2015). Immune cell promotion of metastasis. Nat. Rev. Immunol. *15*, 73–86.

Kobayashi, A., Okuda, H., Xing, F., Pandey, P.R., Watabe, M., Hirota, S., Pai, S.K., Liu, W., Fukuda, K., Chambers, C., et al. (2011). Bone morphogenetic protein 7 in dormancy and metastasis of prostate cancer stem-like cells in bone. J. Exp. Med. *208*, 2641–2655.

Kordes, U., and Hagel, C. (2006). Expression of SOX9 and SOX10 in central neuroepithelial tumor. J. Neurooncol. *80*, 151–155.

Lanier, L.L. (2015). NKG2D receptor and its ligands in host defense. Cancer Immunol. Res. *3*, 575–582.

Li, L., and Clevers, H. (2010). Coexistence of quiescent and active adult stem cells in mammals. Science *327*, 542–545.

Lien, W.H., and Fuchs, E. (2014). Wnt some lose some: transcriptional governance of stem cells by Wnt/β-catenin signaling. Genes Dev. *28*, 1517–1532.

Lim, E., Wu, D., Pal, B., Bouras, T., Asselin-Labat, M.L., Vaillant, F., Yagita, H., Lindeman, G.J., Smyth, G.K., and Visvader, J.E. (2010). Transcriptome analyses of mouse and human mammary cell subpopulations reveal multiple conserved genes and pathways. Breast Cancer Res. *12*, R21.

Liu, S., Cong, Y., Wang, D., Sun, Y., Deng, L., Liu, Y., Martin-Trevino, R., Shang, L., McDermott, S.P., Landis, M.D., et al. (2014). Breast cancer stem cells transition between epithelial and mesenchymal states reflective of their normal counterparts. Stem Cell Reports *2*, 78–91.

Ljunggren, H.G., and Malmberg, K.J. (2007). Prospects for the use of NK cells in immunotherapy of human cancer. Nat. Rev. Immunol. *7*, 329–339.

MacKie, R.M., Reid, R., and Junor, B. (2003). Fatal melanoma transferred in a donated kidney 16 years after melanoma surgery. N. Engl. J. Med. *348*, 567–568.

Maeda, R., Yoshida, J., Hishida, T., Aokage, K., Nishimura, M., Nishiwaki, Y., and Nagai, K. (2010). Late recurrence of non-small cell lung cancer more than 5 years after complete resection: incidence and clinical implications in patient follow-up. Chest *138*, 145–150.

Malanchi, I., Santamaria-Martínez, A., Susanto, E., Peng, H., Lehr, H.A., Delaloye, J.F., and Huelsken, J. (2012). Interactions between cancer stem cells and their niche govern metastatic colonization. Nature *481*, 85–89.

Martinet, L., and Smyth, M.J. (2015). Balancing natural killer cell activation through paired receptors. Nat. Rev. Immunol. *15*, 243–254.

Massagué, J. (2012). TGFβ signalling in context. Nat. Rev. Mol. Cell Biol. *13*, 616–630.

Massagué, J., and Obenauf, A.C. (2016). Metastatic colonization by circulating tumour cells. Nature *529*, 298–306. http://dx.doi.org/10.1038/nature17038.

Nguyen, D.X., Chiang, A.C., Zhang, X.H., Kim, J.Y., Kris, M.G., Ladanyi, M., Gerald, W.L., and Massagué, J. (2009). WNT/TCF signaling through LEF1 and HOXB9 mediates lung adenocarcinoma metastasis. Cell *138*, 51–62.

O'Sullivan, T., Saddawi-Konefka, R., Vermi, W., Koebel, C.M., Arthur, C., White, J.M., Uppaluri, R., Andrews, D.M., Ngiow, S.F., Teng, M.W., et al. (2012). Cancer immunoediting by the innate immune system in the absence of adaptive immunity. J. Exp. Med. *209*, 1869–1882.

Oskarsson, T., Acharyya, S., Zhang, X.H., Vanharanta, S., Tavazoie, S.F., Morris, P.G., Downey, R.J., Manova-Todorova, K., Brogi, E., and Massagué, J. (2011). Breast cancer cells produce tenascin C as a metastatic niche component to colonize the lungs. Nat. Med. *17*, 867–874.

Park, S.B., Seo, K.W., So, A.Y., Seo, M.S., Yu, K.R., Kang, S.K., and Kang, K.S. (2012). SOX2 has a crucial role in the lineage determination and proliferation of mesenchymal stem cells through Dickkopf-1 and c-MYC. Cell Death Differ. *19*, 534–545.

Pelleitier, M., and Montplaisir, S. (1975). The nude mouse: a model of deficient T-cell function. Methods Achiev. Exp. Pathol. *7*, 149–166.

Rudin, C.M., Durinck, S., Stawiski, E.W., Poirier, J.T., Modrusan, Z., Shames, D.S., Bergbower, E.A., Guan, Y., Shin, J., Guillory, J., et al. (2012). Comprehensive genomic analysis identifies SOX2 as a frequently amplified gene in small-cell lung cancer. Nat. Genet. *44*, 1111–1116.

Sarkar, A., and Hochedlinger, K. (2013). The sox family of transcription factors: versatile regulators of stem and progenitor cell fate. Cell Stem Cell *12*, 15–30.

Seo, E., Basu-Roy, U., Gunaratne, P.H., Coarfa, C., Lim, D.S., Basilico, C., and Mansukhani, A. (2013). SOX2 regulates YAP1 to maintain stemness and determine cell fate in the osteo-adipo lineage. Cell Rep. *3*, 2075–2087.

Shultz, L.D., Lyons, B.L., Burzenski, L.M., Gott, B., Chen, X., Chaleff, S., Kotb, M., Gillies, S.D., King, M., Mangada, J., et al. (2005). Human lymphoid and myeloid cell development in NOD/LtSz-scid IL2R gamma null mice engrafted with mobilized human hemopoietic stem cells. J. Immunol. *174*, 6477–6489.

Sojka, D.K., Plougastel-Douglas, B., Yang, L., Pak-Wittel, M.A., Artyomov, M.N., Ivanova, Y., Zhong, C., Chase, J.M., Rothman, P.B., Yu, J., et al. (2014). Tissue-resident natural killer (NK) cells are cell lineages distinct from thymic and conventional splenic NK cells. eLife *3*, e01659.

Sosa, M.S., Bragado, P., and Aguirre-Ghiso, J.A. (2014). Mechanisms of disseminated cancer cell dormancy: an awakening field. Nat. Rev. Cancer *14*, 611–622.

Sun, J.C., and Lanier, L.L. (2008). Cutting edge: viral infection breaks NK cell tolerance to "missing self". J. Immunol. *181*, 7453–7457.

Takeda, K., Smyth, M.J., Cretney, E., Hayakawa, Y., Yamaguchi, N., Yagita, H., and Okumura, K. (2001). Involvement of tumor necrosis factor-related apoptosis-inducing ligand in NK cell-mediated and IFN-gamma-dependent suppression of subcutaneous tumor growth. Cell. Immunol. *214*, 194–200.

Treutlein, B., Brownfield, D.G., Wu, A.R., Neff, N.F., Mantalas, G.L., Espinoza, F.H., Desai, T.J., Krasnow, M.A., and Quake, S.R. (2014). Reconstructing lineage hierarchies of the distal lung epithelium using single-cell RNA-seq. Nature *509*, 371–375.

Valiente, M., Obenauf, A.C., Jin, X., Chen, Q., Zhang, X.H., Lee, D.J., Chaft, J.E., Kris, M.G., Huse, J.T., Brogi, E., and Massagué, J. (2014). Serpins promote cancer cell survival and vascular co-option in brain metastasis. Cell *156*, 1002–1016.

Vesely, M.D., Kershaw, M.H., Schreiber, R.D., and Smyth, M.J. (2011). Natural innate and adaptive immunity to cancer. Annu. Rev. Immunol. *29*, 235–271.

Villegas, F.R., Coca, S., Villarrubia, V.G., Jiménez, R., Chillón, M.J., Jareño, J., Zuil, M., and Callol, L. (2002). Prognostic significance of tumor infiltrating natural killer cells subset CD57 in patients with squamous cell lung cancer. Lung Cancer *35*, 23–28.

Winslow, M.M., Dayton, T.L., Verhaak, R.G., Kim-Kiselak, C., Snyder, E.L., Feldser, D.M., Hubbard, D.D., DuPage, M.J., Whittaker, C.A., Hoersch, S., et al. (2011). Suppression of lung adenocarcinoma progression by Nkx2-1. Nature *473*, 101–104.

Wu, J., and Lanier, L.L. (2003). Natural killer cells and cancer. Adv. Cancer Res. *90*, 127–156.

Xiao, D., Craig, J.C., Chapman, J.R., Dominguez-Gil, B., Tong, A., and Wong, G. (2013). Donor cancer transmission in kidney transplantation: a systematic review. Am. J. Transplant. *13*, 2645–2652.

Zhang, X.H., Wang, Q., Gerald, W., Hudis, C.A., Norton, L., Smid, M., Foekens, J.A., and Massagué, J. (2009). Latent bone metastasis in breast cancer tied to Src-dependent survival signals. Cancer Cell *16*, 67–78.

A

AdenoCa	Cell Line	Source	Mutations	Lines (Organs)
Lung	H2087	Stage I Lymph Node	$NRAS^{Q61K}$ $BRAF^{L597V}$ $p53^{V157F}$	LCC1 (Lung) LCC2 (Kidney)
Breast	HCC1954	Stage IIA Ductal Lesion	$ERBB2^{Amp}$ $PI3K^{H1047R}$ $p53^{Y163C}$	LCC1 (Brain) LCC2 (Brain)

B

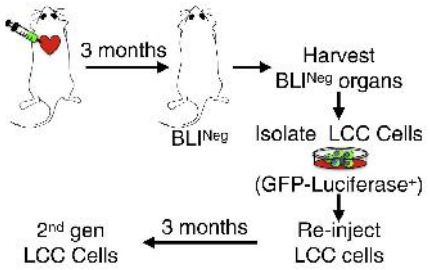

C

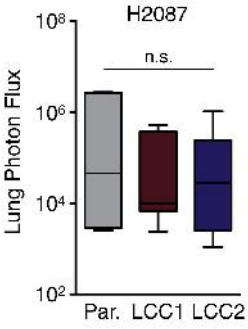

D

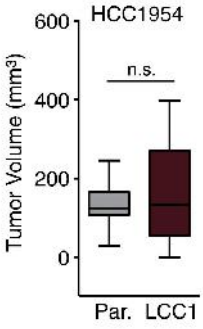

E

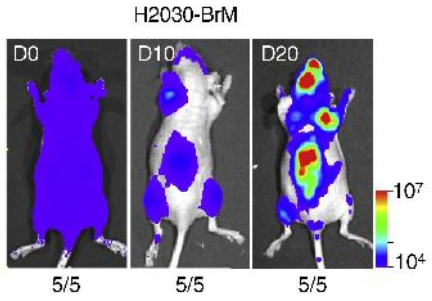

F

BLI^Neg mice with LCC cells	
H2087-Parental	1/7
H2087-LCC1	5/6
H2087-LCC2	10/13
HCC1954-Parental	1/7
HCC1954-LCC1	5/7

G

BLI^Neg mice with LCC cells	
H2087-LCC-M1	3/5
H2087-LCC-M2	2/5
HCC1954-LCC-M1	3/5

H

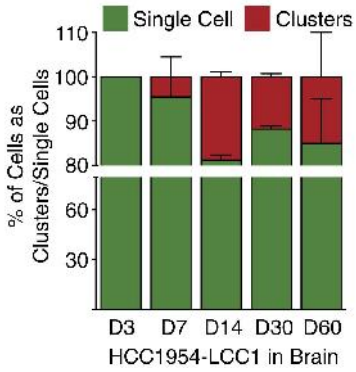

I

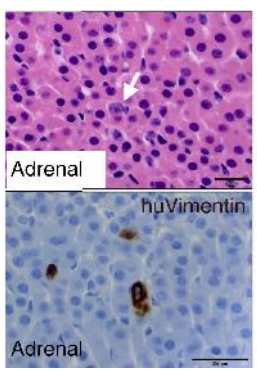

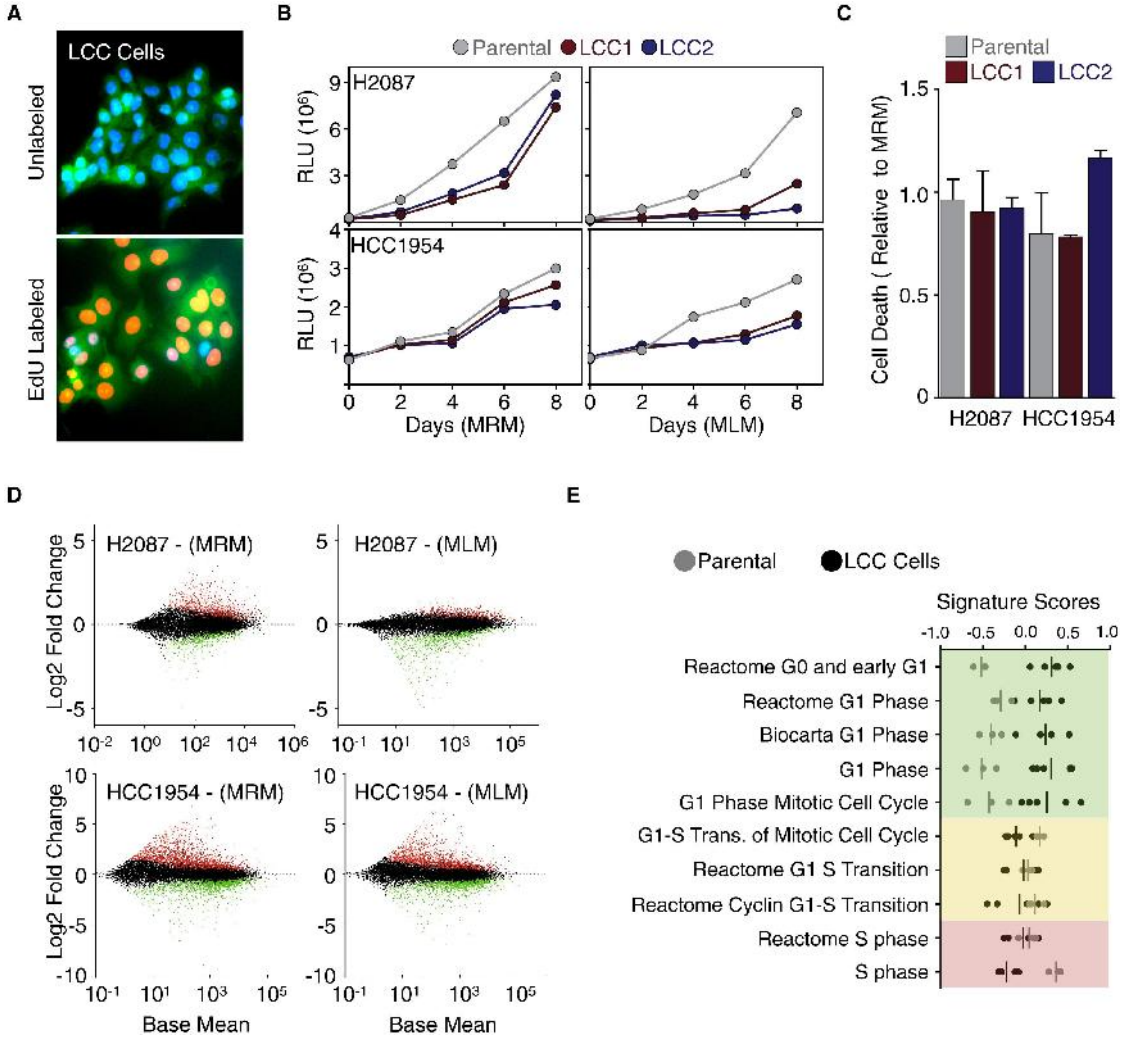
A
LCC Cells
Unlabeled
EdU Labeled
B
Parental
LCC1
LCC2
H2087
HCC1954
RLU (10^6)
Days (MRM)
Days (MLM)
C
Parental
LCC1
LCC2
Cell Death (Relative to MRM)
H2087
HCC1954
D
H2087 - (MRM)
H2087 - (MLM)
HCC1954 - (MRM)
HCC1954 - (MLM)
Log2 Fold Change
Base Mean
E
Parental
LCC Cells
Signature Scores
Reactome G0 and early G1
Reactome G1 Phase
Biocarta G1 Phase
G1 Phase
G1 Phase Mitotic Cell Cycle
G1-S Trans. of Mitotic Cell Cycle
Reactome G1 S Transition
Reactome Cyclin G1-S Transition
Reactome S phase
S phase

A

Gene Set	N.E.S	FDR q-val
Br. Ca 20q12-q13	5.68	<0.0001
HCP - H3K27me3	4.37	<0.0001
Hu ES SUZ12 targets	3.9	<0.0001
Mammary Stem Cell	**3.89**	**<0.0001**
HCP - HK327me3	3.8	<0.0001
Colorectal Adenoma	3.7	<0.0001

B

Cell Line	% Engraftment Cells per injections 100K	10K	1K
H2087 - Par.	100	50.0	8.3
H2087 - LCC1	100	58.3	33.3
H2087 - LCC2	100	75.0	25.0
HCC1954 - Par.	100	33.3	0.0
HCC1954 - LCC1	100	66.7	16.7

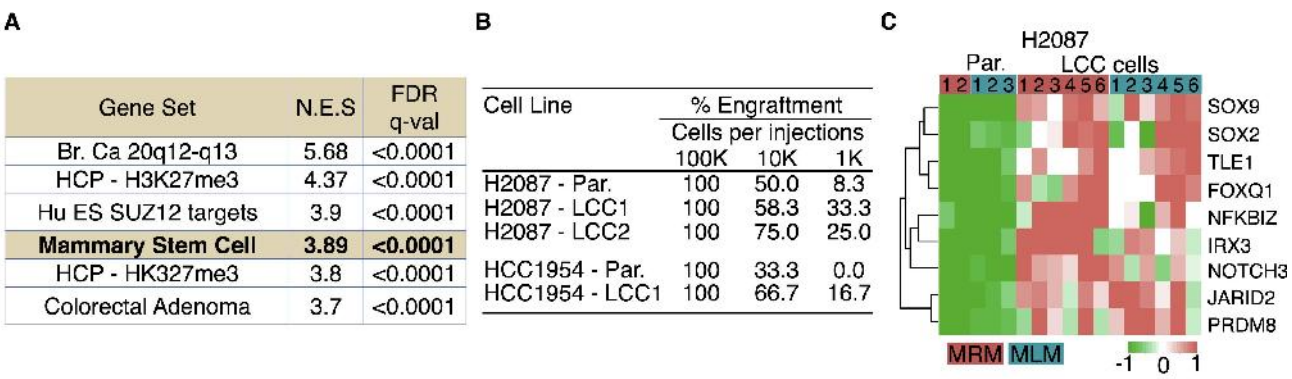

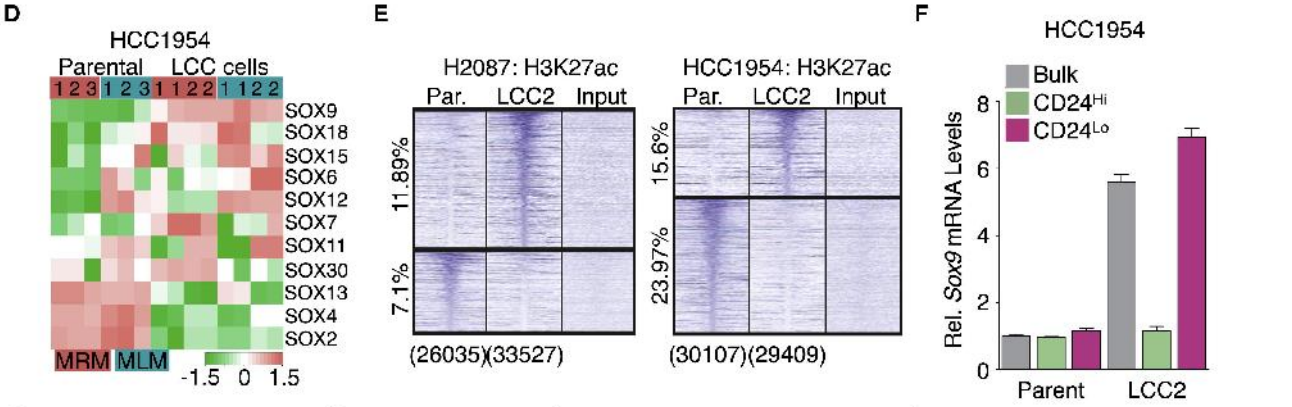

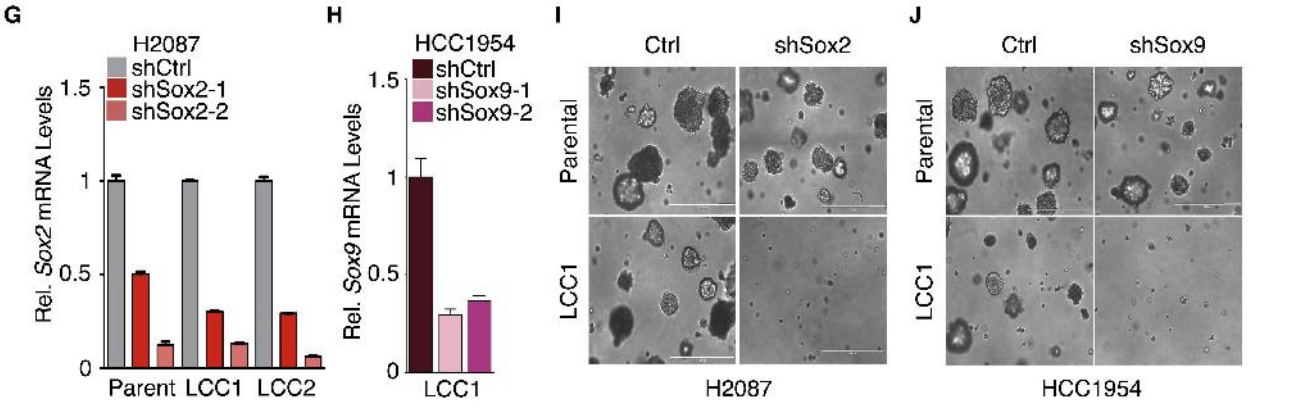

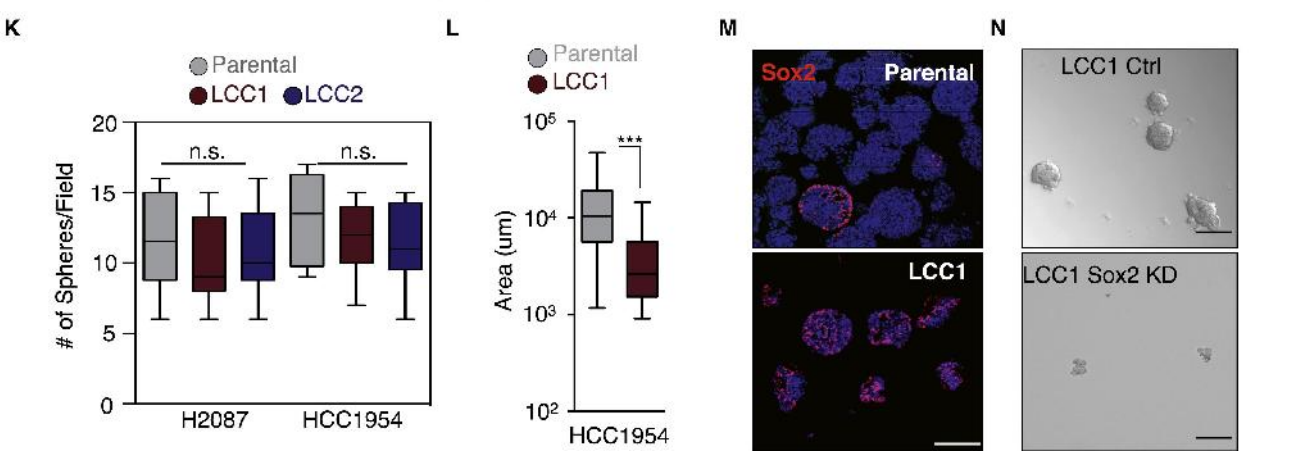

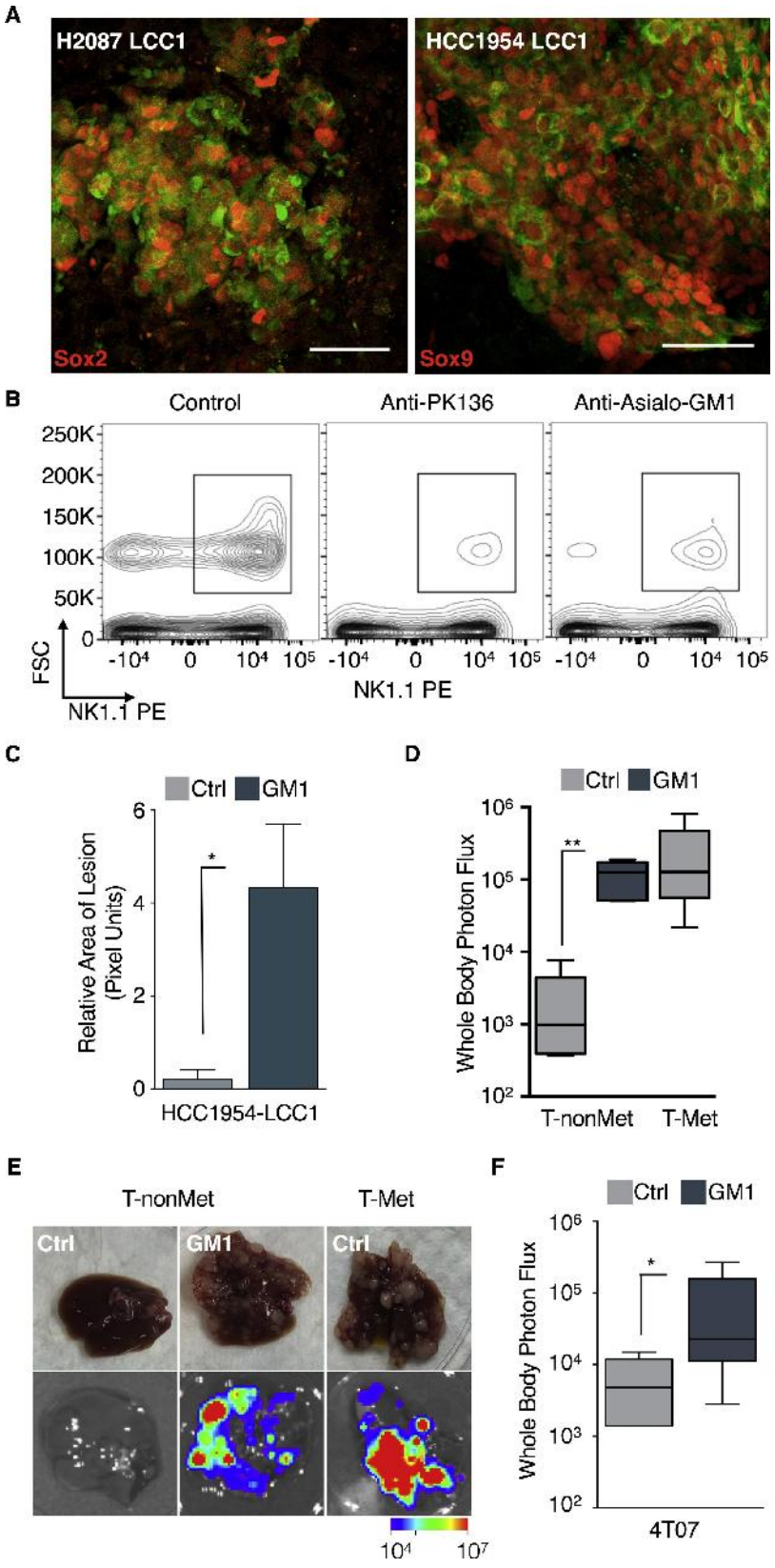
A
H2087 LCC1
Sox2
HCC1954 LCC1
Sox9
B
Control
Anti-PK136
Anti-Asialo-GM1
250K
200K
150K
100K
50K
0
FSC
NK1.1 PE
-10⁴
0
10⁴
10⁵
NK1.1 PE
C
Ctrl
GM1
Relative Area of Lesion (Pixel Units)
6
4
2
0
*
HCC1954-LCC1
D
Ctrl
GM1
Whole Body Photon Flux
10⁶
10⁵
10⁴
10³
10²
**
T-nonMet
T-Met
E
T-nonMet
T-Met
Ctrl
GM1
Ctrl
10⁴
10⁷
F
Ctrl
GM1
Whole Body Photon Flux
10⁶
10⁵
10⁴
10³
10²
*
4T07

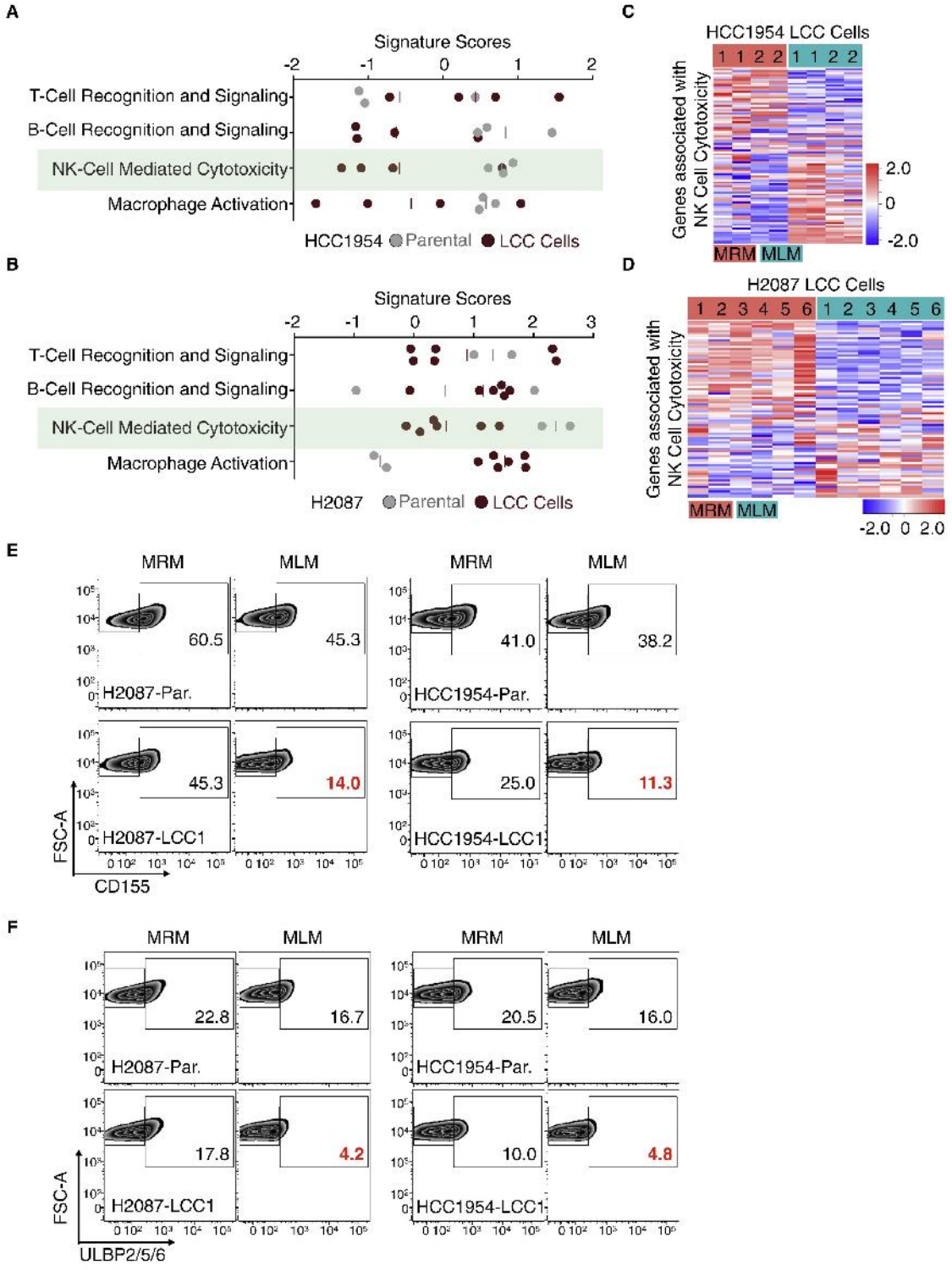
A
Signature Scores
-2 -1 0 1 2
T-Cell Recognition and Signaling
B-Cell Recognition and Signaling
NK-Cell Mediated Cytotoxicity
Macrophage Activation
HCC1954 Parental LCC Cells
B
Signature Scores
-2 -1 0 1 2 3
T-Cell Recognition and Signaling
B-Cell Recognition and Signaling
NK-Cell Mediated Cytotoxicity
Macrophage Activation
H2087 Parental LCC Cells
C
HCC1954 LCC Cells
1 1 2 2 1 1 2 2
Genes associated with NK Cell Cytotoxicity
2.0
0
-2.0
MRM MLM
D
H2087 LCC Cells
1 2 3 4 5 6 1 2 3 4 5 6
Genes associated with NK Cell Cytotoxicity
MRM MLM
-2.0 0 2.0
E
MRM MLM MRM MLM
60.5 45.3 41.0 38.2
H2087-Par. HCC1954-Par.
45.3 14.0 25.0 11.3
H2087-LCC1 HCC1954-LCC1
FSC-A
CD155
F
MRM MLM MRM MLM
22.8 16.7 20.5 16.0
H2087-Par. HCC1954-Par.
17.8 4.2 10.0 4.8
H2087-LCC1 HCC1954-LCC1
FSC-A
ULBP2/5/6

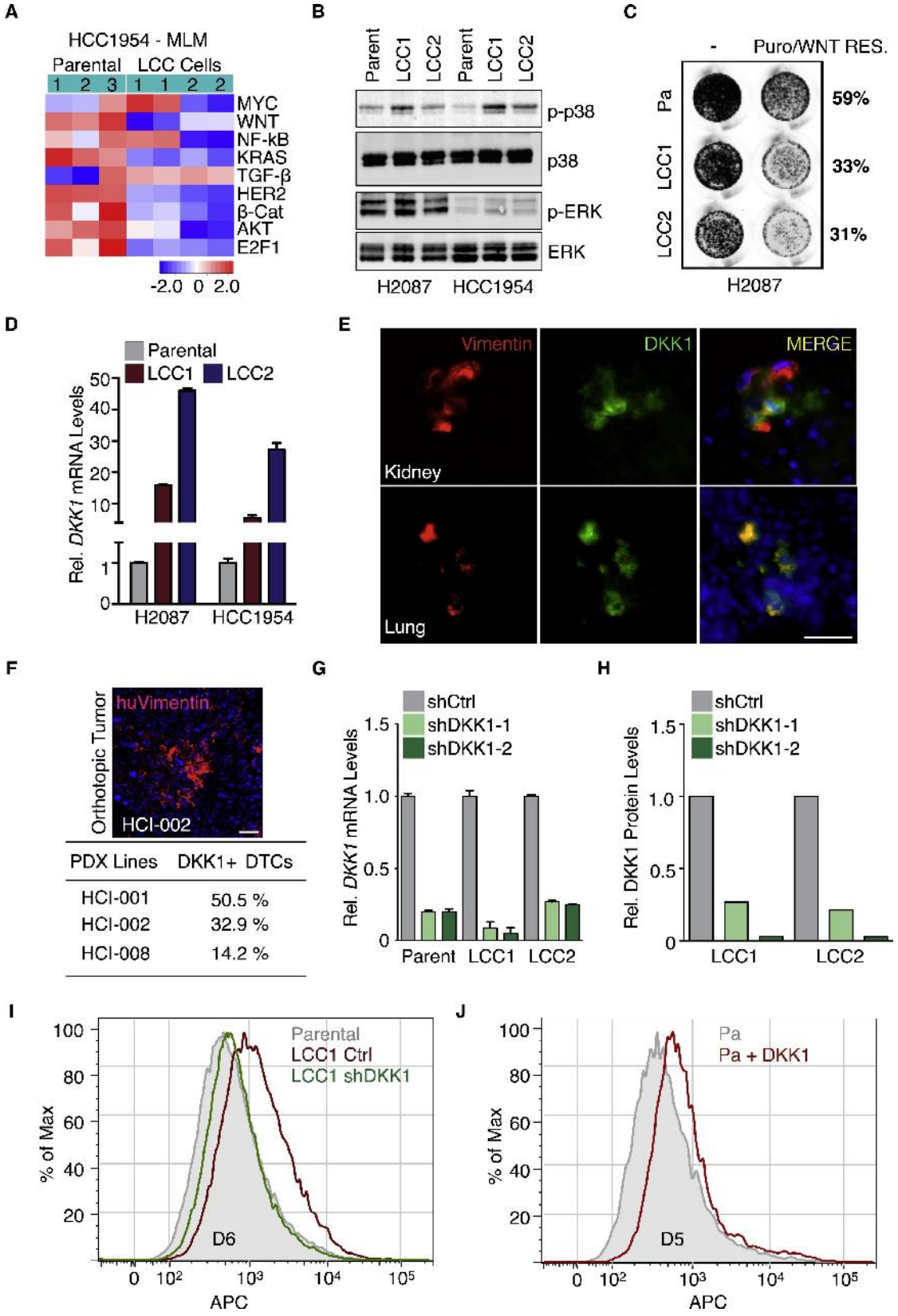
A
HCC1954 - MLM
Parental
LCC Cells
1 2 3 1 1 2 2
MYC
WNT
NF-kB
KRAS
TGF-β
HER2
β-Cat
AKT
E2F1
-2.0 0 2.0
B
Parent
LCC1
LCC2
Parent
LCC1
LCC2
p-p38
p38
p-ERK
ERK
H2087
HCC1954
C
-
Puro/WNT RES.
Pa
LCC1
LCC2
59%
33%
31%
H2087
D
Parental
LCC1
LCC2
Rel. DKK1 mRNA Levels
50
40
30
20
10
1
0
H2087
HCC1954
E
Vimentin
DKK1
MERGE
Kidney
Lung
F
Orthotopic Tumor
huVimentin
HCI-002
PDX Lines
DKK1+ DTCs
HCI-001
50.5 %
HCI-002
32.9 %
HCI-008
14.2 %
G
shCtrl
shDKK1-1
shDKK1-2
Rel. DKK1 mRNA Levels
1.5
1.0
0.5
0
Parent
LCC1
LCC2
H
shCtrl
shDKK1-1
shDKK1-2
Rel. DKK1 Protein Levels
1.5
1.0
0.5
0
LCC1
LCC2
I
Parental
LCC1 Ctrl
LCC1 shDKK1
% of Max
100
80
60
40
20
D6
0
10²
10³
10⁴
10⁵
APC
J
Pa
Pa + DKK1
% of Max
100
80
60
40
20
D5
0
10²
10³
10⁴
10⁵
APC

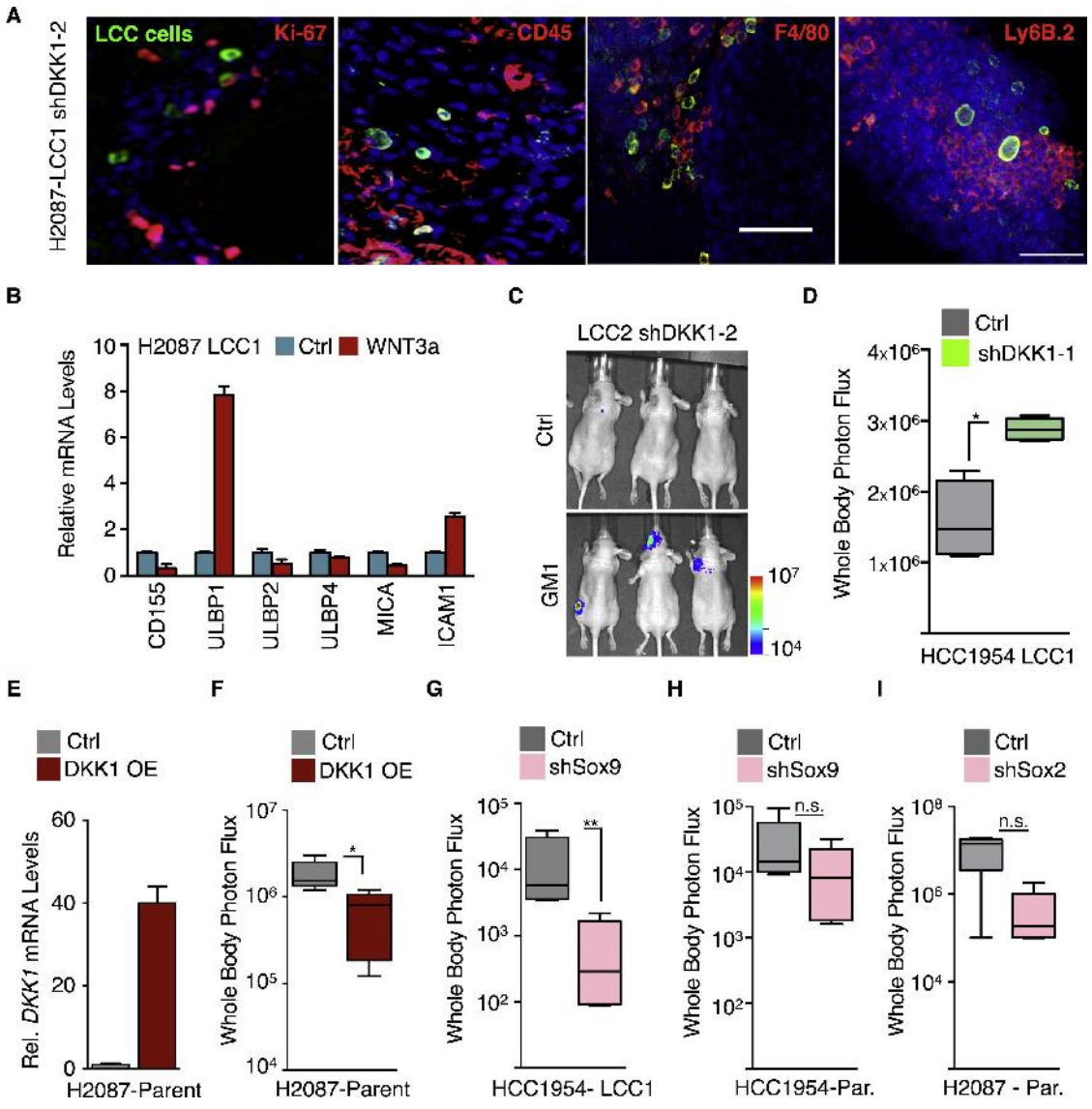
A
H2087-LCC1 shDKK1-2
LCC cells
Ki-67
CD45
F4/80
Ly6B.2
B
H2087 LCC1
Ctrl
WNT3a
Relative mRNA Levels
CD155
ULBP1
ULBP2
ULBP4
MICA
ICAM1
C
LCC2 shDKK1-2
Ctrl
GM1
D
Ctrl
shDKK1-1
Whole Body Photon Flux
HCC1954 LCC1
E
Ctrl
DKK1 OE
Rel. DKK1 mRNA Levels
H2087-Parent
F
Ctrl
DKK1 OE
Whole Body Photon Flux
H2087-Parent
G
Ctrl
shSox9
Whole Body Photon Flux
HCC1954- LCC1
H
Ctrl
shSox9
Whole Body Photon Flux
n.s.
HCC1954-Par.
I
Ctrl
shSox2
Whole Body Photon Flux
n.s.
H2087 - Par.